Identifying loci under selection via explicit demographic models

Hirzi Luqman[1*], Alex Widmer[1], Simone Fior[1†], Daniel Wegmann[2,3†*]

[1] Institute of Integrative Biology, ETH Zurich, Universitätstrasse 16, 8092 Zürich, Switzerland

[2] Department of Biology, University of Fribourg, Fribourg, Switzerland

[3] Swiss Institute of Bioinformatics, Fribourg, Switzerland

† denotes joint senior authors

Corresponding authors: hirzi.luqman@env.ethz.ch and daniel.wegmann@unifr.ch

Abstract

Adaptive genetic variation is a function of both selective and neutral forces. To accurately identify adaptive loci, it is thus critical to account for demographic history. Theory suggests that signatures of selection can be inferred using the coalescent, following the premise that genealogies of selected loci deviate from neutral expectations. Here, we build on this theory to develop an analytical framework to identify Loci under Selection via explicit Demographic models (LSD). Under this framework, signatures of selection are inferred through deviations in demographic parameters, rather than through summary statistics directly, and demographic history is accounted for explicitly. Leveraging on the property of demographic models to incorporate directionality, we show that LSD can provide information on the environment in which selection acts on a population. This can prove useful in elucidating the selective processes underlying local adaptation, by characterising genetic trade-offs and extending the concepts of antagonistic pleiotropy and conditional neutrality from ecological theory to practical application in genomic data. We implement LSD via Approximate Bayesian Computation and demonstrate, via simulations, that LSD has i) high power to identify selected loci across a large range of demographic-selection regimes, ii) outperforms commonly applied genome-scan methods under complex demographies, and iii) accurately infers the directionality of selection for identified candidates. Using the same simulations, we further characterise the behaviour of isolation-with-migration models conducive to the study of local adaptation under regimes of selection. Finally, we demonstrate an application of LSD by detecting loci and characterising genetic trade-offs underlying flower colour in *Antirrhinum majus*.

Keywords

Approximate Bayesian computation, demography, genetic trade-offs, genome scan, local adaptation, selection

1 INTRODUCTION

Elucidating the genetic basis of adaptation and identifying genetic determinants of population and species divergence are key foci in evolutionary biology. In natural systems, genetic variation is shaped by the demographic history (driven by the neutral processes of mutation, migration and drift) together with natural selection on loci underlying adaptive traits. While all gene genealogies are constrained by the demographic history of the population, the genealogies of loci affected by selection are perturbed and may differ in key characteristics compared to those evolving under neutrality, though converging patterns can arise (Bierne, Welch, Loire, Bonhomme, & David, 2011; Edmonds, Lillie, & Cavalli-Sforza, 2004; Laurent Excoffier, Foll, & Petit, 2009; J. Li et al., 2012; Montgomery Slatkin & Excoffier, 2012). Disentangling the genomic signatures generated by these two processes, i.e. correctly identifying adaptive loci, remains a prevailing challenge in the field of population genetics (Biswas & Akey, 2006; Horscroft, Ennis, Pengelly, Sluckin, & Collins, 2019; Luikart, England, Tallmon, Jordan, & Taberlet, 2003).

A multitude of methods have been developed that identify loci under selection as those whose summary statistics deviate from the genome-wide distribution. These "outlier" approaches can generally be grouped into three classes: those that 1) detect regions of elevated differentiation between populations (via e.g. F_{ST}-related statistics), 2) detect regions of

perturbed site frequency spectrum (SFS) via diversity or diversity-related estimators (e.g. π, Tajima's *D*) and 3) detect regions of extensive linkage disequilibrium (LD) via haplotype statistics (e.g. EHH, iHS) (M. A. Beaumont & Nichols, 1996; Biswas & Akey, 2006; Luikart et al., 2003; Oleksyk, Smith, & O'Brien, 2010; Sabeti et al., 2002; Vitti, Grossman, & Sabeti, 2013). While in empirical studies inference of selection is often achieved through corroboratory evidence from multiple measures, the choice of a particular class and hence summary statistic is motivated by the type of selection one aims to infer; with the first geared towards divergent selection between populations and the others towards footprints of selection within single populations.

Under the premise that adaptive genetic variation is a function of both selective and neutral forces, accounting for the demographic history of the study system is critical for the correct identification of selected loci (L. Excoffier, Hofer, & Foll, 2009; François, Martins, Caye, & Schoville, 2016; Hoban et al., 2016; Hofer, Ray, Wegmann, & Excoffier, 2009). This is commonly achieved by contrasting locus-specific statistics against an estimate of the expected distribution of these statistics under demography alone, with the power of such an approach being a function of both the summary statistics used and the accuracy with which the neutral distribution is inferred. In the context of identifying local adaptation, the canonical statistics employed is F_{ST}, and the first methods to infer its neutral distribution used simulations under an island model calibrated by matching the observed heterozygosity at each locus (M. A. Beaumont & Nichols, 1996; L. Excoffier et al., 2009). Under island models, the distribution of sample allele frequencies is also well captured by Pólya distributions (Balding & Nichols, 1994; Rannala & Hartigan, 1996), which can be learned using likelihood-based

methods that jointly classify loci into neutral and selected classes (Mark A. Beaumont & Balding, 2004; Foll & Gaggiotti, 2008; Galimberti et al., 2020). While generally powerful, these methods suffer from high false-positive rates in the case of asymmetric divergence between populations (Galimberti et al., 2020; Lotterhos & Whitlock, 2014; Luu, Bazin, & Blum, 2017), which violates a key assumption of island models. This can be alleviated by using hierarchical island models (Foll, Gaggiotti, Daub, Vatsiou, & Excoffier, 2014; Galimberti et al., 2020) or a more flexible distribution to capture neutral allele frequencies (e.g. PCA, Luu, Bazin, & Blum, 2017). For some natural systems however, these approaches may still be insufficient to capture the demographic history of the population and a (potentially complex) demographic model should be used. Williamson et al. (2005), for instance, inferred such a model from putatively neutral loci and then identified loci under selection as those for which an additional selection parameter is required.

Rather than modelling selection explicitly, loci under selection may also be identified under pure demographic models through locus-specific demographic parameters, under the premise that the demographic parameters of selected loci are expected to deviate from neutral expectations (Barton & Bengtsson, 1986; Charlesworth, 2009; Charlesworth, Nordborg, & Charlesworth, 1997; Fusco & Uyenoyama, 2011; Galtier, Depaulis, & Barton, 2000; Gossmann, Woolfit, & Eyre-Walker, 2011; Petry, 1983; Sousa, Carneiro, Ferrand, & Hey, 2013). Under coalescent theory, demographic models are parametrized by the effective sizes (N_E) of each population and the effective rates of migration (M_E) between them, which respectively describe the level of drift and gene flow within and between populations (Charlesworth, 2009; Petry, 1983). Importantly, both N_E and M_E may change through time.

106 Different modes of selection and adaptive processes can be expected to alter these
107 demographic parameters in different ways. In a single population, a selective sweep is
108 expected to reduce N_E at selected and linked sites while diversifying selection is expected to
109 increase it (Galtier et al., 2000; Gossmann et al., 2011). In the case of two or more
110 populations connected by gene flow, balancing selection and adaptive introgression are
111 expected to increase M_E at selected and linked sites, while divergent selection is expected to
112 reduce M_E at those sites (Charlesworth et al., 1997; Geraldes, Ferrand, & Nachman, 2006;
113 Petry, 1983; Won, Sivasundar, Wang, & Hey, 2005).
114
115 Notably, locus-specific demographic parameters are not just informative about the
116 strength (i.e. the magnitude of variation in N_E or M_E) and mode of selection (i.e. a reduction
117 or elevation of N_E or M_E), but may also identify the population (or environment) in which
118 selection acts (i.e. a reduction in M_E in one but not the other direction). Directional selection
119 modulates fitness of natural populations by purging maladaptive alleles via extrinsic barriers
120 such as hybrid or immigrant inviability, or lower fecundity (Naisbit, Jiggins, & Mallet, 2001;
121 Nosil, Vines, & Funk, 2005; Rundle & Whitlock, 2001; Schluter, 2000). This effectively
122 reduces M_E at selected loci proportionally to the strength of selection (Petry, 1983). Under
123 local adaptation, alternate alleles may confer higher fitness in their respective local
124 environment but reduced fitness in the foreign environment, i.e. antagonistic pleiotropy (AP),
125 or an allele may confer higher fitness in its local environment but have no differential effect
126 relative to the alternative allele in the foreign environment, i.e. conditional neutrality (CN)
127 (Anderson, Lee, Rushworth, Colautti, & Mitchell-Olds, 2013; Kawecki & Ebert, 2004;
128 Savolainen, Lascoux, & Merilä, 2013). To date, such genetic trade-offs have only been

129 characterized in a handful of cases, primarily through demanding experiments involving the
130 transplanting of alternate genotypes in their reciprocal environments (Anderson, Lee, &
131 Mitchell-Olds, 2014; Anderson et al., 2013; Oakley, Ågren, Atchison, & Schemske, 2014;
132 Troth, Puzey, Kim, Willis, & Kelly, 2018). Characterizing the nature of such trade-offs
133 directly from genomic data presents a promising complementary approach, applicable to
134 natural populations, to investigate the genetic basis of local adaptation, a key concept in
135 ecological genetics.
136
137 Inferring demographic parameters using coalescent theory is, however, computationally
138 challenging, as the underlying but unknown genealogies must be integrated out numerically
139 (Hey & Nielsen, 2007). As a result, there exists only a single likelihood implementation to
140 infer locus-specific and global demographic parameters jointly: an MCMC sampler that
141 attributes loci to different classes (e.g. selected and neutral) and jointly infers the demographic
142 parameters of a two-population isolation-with-migration (IM) model for each group (Sousa
143 et al., 2013). To extend this approach to more complex models, simulation-based techniques
144 such as Approximate Bayesian Computation (Mark A. Beaumont, Zhang, & Balding, 2002;
145 Marjoram & Tavaré, 2006; Sisson, Fan, & Beaumont, 2018) may be employed. The use of
146 ABC to infer genome-wide demographic parameters has a long tradition (e.g. Dussex,
147 Wegmann, & Robertson, 2014; Wegmann & Excoffier, 2010) and it may also be used to
148 infer locus-specific parameters in a hierarchical setting, but it is computationally challenging.
149 Indeed, the dimensionality of a genome-wide model is prohibitively large for any naïve
150 Monte-Carlo scheme as the probability that a simulation matches the data at all loci is
151 virtually zero. When inferring genome-wide parameters, loci are exchangeable and this

problem is easily overcome by using summary statistics that are functions of all loci such as the (scaled) moments of the distribution of locus-specific statistics (Tavaré, Balding, Griffiths, & Donnelly, 1997; Wegmann, Leuenberger, & Excoffier, 2009). To benefit from this in a hierarchical setting, Bazin *et al.* (2010) proposed a two-step algorithm in which hierarchical parameters are inferred based on moments of locus-specific summary statistics, and locus-specific parameters are then inferred with simulations of a single locus conducted with parameters drawn from the posterior distribution of the hierarchical parameters. As recently shown (Kousathanas, Leuenberger, Helfer, Quinodoz, & Foll, 2016), this approach can be generalized to arbitrary parameter dependencies when using an ABC-MCMC setting that also eliminates the need for a two-step approach. These approaches were successfully used to infer locus-specific (Bazin, Dawson, & Beaumont, 2010) and cluster-specific (Aeschbacher, Futschik, & Beaumont, 2013) migration rates, as well as locus-specific selection coefficients (Foll, Poh, et al., 2014; Kousathanas et al., 2016) for up to several hundred loci. Scaling such inference up to whole-genomes, however, remains difficult due to the requirement to simulate all loci.

In this paper, we introduce LSD, an alternative framework for identifying Loci under Selection via explicit Demographic models that scales to genomic data. Similar to the approach by Bazin *et al.* (2010), LSD works in two steps. But rather than inferring hierarchical parameters for all loci, LSD first obtains a point estimate of demographic parameters for neutral loci, which is then compared against per-locus estimates to identify selected loci. This has the benefit of requiring only simulations of a single locus, which can be efficiently recycled (Thalmann et al., 2011). As a downside, the approach requires *a priori*

knowledge on putative neutral sites. However, as we show with simulations, the approach is very robust to mis-specifications.

While LSD is flexible regarding the choice of demographic model and can in principle accommodate any discrete population model (including single population and stepping-stone models) as well as detect different modes of selection, we demonstrate here LSD's utility in studies of local adaptation by focusing on the detection of loci under divergent selection between populations under isolation-with-migration (IM) models. We validate and assess the performance of LSD via extensive simulations, provide general insights into the properties of IM models in relation to the power of LSD and other widely applied genome scan methods, and demonstrate an application of the method to the detection of functionally validated loci underlying flower colour in two parapatric subspecies of *Antirrhinum majus* (common snapdragon) (Schwinn et al., 2006; Tavares et al., 2018).

2 MATERIALS AND METHODS

2.1 Model

We begin by outlining the conceptual framework underlying LSD. Consider a demographic model $\boldsymbol{\mathcal{M}}$, parameterized by demographic parameters $\boldsymbol{\theta}$, that generates genetic data $\boldsymbol{D}$. To quantify deviations from neutrality, LSD first estimates the demographic parameters $\widehat{\boldsymbol{\theta}}$ from a collection of loci assumed to be neutral (Figure S1). In a second step, LSD performs demographic inference on all loci and determines the posterior distribution $\pi_l(\boldsymbol{\theta}) = \pi(\boldsymbol{\theta}|\boldsymbol{D_l})$ for each locus. Finally, LSD assesses the concordance of $\widehat{\boldsymbol{\theta}}$ with $\pi_l(\boldsymbol{\theta})$ by determining h_l, the highest posterior density interval (HPDI) of $\boldsymbol{\pi_l}(\boldsymbol{\theta})$ that contains $\widehat{\boldsymbol{\theta}}$, and

uses $p_l = 1 - h_l$ as a metric to identify locus l as incompatible with $\widehat{\boldsymbol{\theta}}$. For loci with parameters $\widehat{\boldsymbol{\theta}}$, p_l follows a uniform distribution (the coverage property) and is interpreted as a p-value to reject $\widehat{\boldsymbol{\theta}}$ for locus l. The joint posterior distribution $\pi_l(\boldsymbol{\theta})$ may further provide information on the magnitude and directionality of selection.

Given that the evaluation of the likelihood is non-trivial and may be intractable under more complex models, we resort to an approximate approach (Marjoram & Tavaré, 2006) (Figure 1). Under an Approximate Bayesian Computation (ABC) framework, the likelihood is approximated by simulations, the outcomes of which are compared with observed data in terms of summary statistics. That is, we find the set of parameters $\boldsymbol{\theta}$ that minimise the distance between the observed data $\boldsymbol{D}$ and the simulated data $\boldsymbol{D}'$. To efficiently evaluate this, we reduce the dimensionality of the data via summarising them into a set of lower-dimensional summary statistics $\boldsymbol{S}$ and $\boldsymbol{S}'$, which are selected to capture the relevant information in $\boldsymbol{D}$ and $\boldsymbol{D}'$, respectively (Mark A. Beaumont et al., 2002; Joyce & Marjoram, 2008; Sisson et al., 2018).

An appropriate model for generating simulated genetic data is provided by coalescent theory (Kingman, 1982; Wakeley, 2001), parametrised by population demographic parameters $\boldsymbol{\theta} = \{\boldsymbol{N_E}, \boldsymbol{M_E}, \mu\}$, where $\boldsymbol{N_E}$ refers to the vector of effective population sizes, $\boldsymbol{M_E}$ to the vector of effective migration rates, and μ to the mutation rate. We stress that population sizes and migration rates may vary through time.

2.2 Implementation

221 We implemented the framework described above as shown in Figure 1 and detailed
222 below.
223
224 **Simulations.** While the framework is readily used for any type of locus, we consider
225 here a locus to consist of a genomic window with a shared genealogy. This effectively implies
226 that recombination is free between loci and fixed within. We simulate genealogies using
227 msms (Ewing & Hermisson, 2010), under a user-defined demographic model. The
228 processing, format and final output of observed genetic data will often differ from that of
229 coalescent simulations, given that observed genetic data may be subject to various pre-
230 sequencing (e.g. pooling), sequencing (e.g. sequencing errors, stochastic sampling of reads)
231 and post-sequencing (e.g. filters) events that perturb and reformat the data from the original
232 source. We thus implement two complementary programs that interface with coalescent
233 simulators to replicate observed sequencing pipelines and generate simulated sequencing data:
234 *LSD-High* can accommodate and simulate both individual and pooled data and assumes mid
235 to high coverage (>10x) data, while *LSD-Low* accepts individual data and can additionally
236 accommodate low coverage (>2x) data by utilising genotype likelihoods via msToGLF and
237 ANGSD (Korneliussen, Albrechtsen, & Nielsen, 2014). A suite of summary statistics is then
238 calculated for the simulated and observed data via the same programs. Summary statistics
239 currently implemented include the number of segregating sites (S), private S, nucleotide
240 diversity (π), Watterson's estimator (θ_W), Tajima's D (θ_D), relative divergence (F_{ST}), absolute
241 divergence (D_{XY}), and site frequencies. In principle any summary statistic can be included,
242 contingent on the data and appropriate additions to the programs' scripts. To account for

potential correlation between summary statistics and to retain only their informative components, we apply a Partial Least Squares transformation (Wegmann et al., 2009).

ABC Inference. The estimation of demographic parameters is performed with ABCtoolbox (Wegmann, Leuenberger, Neuenschwander, & Excoffier, 2010), via the ABC-GLM algorithm using the subset of *n* simulations closest to the observed summary statistics. In a first step, LSD infers demographic parameters of putatively neutral loci to obtain the point estimate $\widehat{\boldsymbol{\theta}}$. We do so based on simulations of a single locus. In contrast to classic ABC regression approaches, ABC-GLM can readily use such simulations to accurately infer posterior distributions from many loci as it approximates the likelihood function, rather than the posterior distribution (Thalmann et al., 2011). However, we propose a slightly different approach that does not characterize the full posterior distribution, but we found to result in point estimates $\widehat{\boldsymbol{\theta}}$ that are more accurate (Supplementary Text S4, Figures S1 and S2) and robust to misidentification of putatively neutral loci (Supplementary Text S5, Figures 4 and S3). Specifically, we first infer locus-specific posterior distributions $\pi_l(\boldsymbol{\theta})$ for each putatively neutral locus with ABC-GLM, then calculate the product of these densities $\pi(\boldsymbol{\theta}) = \prod_l \pi_l(\boldsymbol{\theta})$, and identify $\hat{\theta} = \underset{\theta}{\operatorname{argmax}}\, \pi(\theta)$.

In a second step, LSD infers locus-specific posterior distributions using ABC-GLM on all loci, either using the same set of simulations as in the first step, or from simulations of a single locus conducted under the parameters $\widehat{\boldsymbol{\theta}}$, except for the parameters affected by selection (e.g. M_E).

2.3 Simulations

To test the performance of the LSD implementation, we simulated pseudo-observed genomes using the program msms under different demographic and selection parameter values, focusing on IM models relevant for the characterisation of local adaptation. We assumed a diploid system, a common mutation rate $\mu = 5 \times 10^{-7}$ per bp per generation, and all loci to be biallelic with ancestral allele *a* and derived allele *A*. Each simulated pseudo-genome comprised $n_n = 1{,}000$ neutral loci and $n_s = 50$ selected loci of 5kb length, for a total (pseudo-genome) size of 5.25Mb.

Demography We simulated four models representing different levels of complexity in terms of population structure and demographic history (Figure 2, Supplementary Text S1). In all models, selection is inferred from the reciprocal scaled migration rates between two contrasting environments (M_{12}, M_{21}; where $M_E = Nm_E$). We used neutral migration rates $M_{12} = M_{21} = M = 0.5$, 5 and 50 migrants per generation and inferred selection as deviations from these rates. We use model $\boldsymbol{\mathcal{M}_1}$ to represent a simplified, generalised model of local adaptation, model $\boldsymbol{\mathcal{M}_2}$ to represent a more complex case of local adaptation comprising multiple, structured populations, model $\boldsymbol{\mathcal{M}_3}$ to reflect a scenario typical of glacial-induced secondary contact population dynamics and model $\boldsymbol{\mathcal{M}_4}$ to represent a case of hierarchical divergence with complex demography. The specific parameter choices for all models are given in Supplementary Text S1.

Selection To simulate genetic trade-offs, selection was simulated on alternate alleles in the contrasting environments, on top of the demographic model. Specifically, we assumed the

289 beneficial alleles to be dominant such that the relative fitness was $1 + s_1, 1, 1$ and $1, 1, 1 + s_2$
290 for the three genotypes *AA*, *Aa* and *aa* in the demes or meta-populations occupying the two
291 environments, respectively. For the selection coefficients s_1 and s_2, we used all combinations
292 of 0, 0.001, 0.01 and 0.1 and thus included cases of conditional neutrality (CN), in which
293 either $s_1 > 0$, $s_2 = 0$ or $s_1 = 0$, $s_2 > 0$, as well as cases of antagonistic pleiotropy (AP) with
294 $s_1 > 0$, $s_2 > 0$. CN regimes are by definition always asymmetric, while AP regimes can be
295 either symmetric ($s_1 = s_2$) and asymmetric ($s_1 \neq s_2$). We further varied the time of the onset
296 of selection from $T_S = 400$, 4,000, 40,000 and 400,000 generations ago.
297
298 For all models, we considered selection on standing variation with the initial frequency
299 of the derived allele at $f_1 = f_2 = 0.1$ in all demes. For model $\boldsymbol{\mathcal{M}_1}$, we additionally
300 investigated the case of *de-novo* mutations with initial frequencies $f_1 = ½\, N_1$ and $f_2 = 0$.
301 These two cases represent the often-considered starting points for local adaptation (Peter,
302 Huerta-Sanchez, & Nielsen, 2012). Depending on the selection regime and due to the
303 stochasticity of drift, the derived allele *A* may sometimes be lost and hence be absent in the
304 simulation of selected loci (especially in the *de-novo* case). Because such a scenario contains no
305 signal for detection of selection, we excluded such simulations (via the -SFC parameter in
306 msms).
307
308 **Assessing accuracy** We inferred selection by contrasting the locus-specific migration
309 rates M_{12} and M_{21} against their neutral estimates $\widehat{M}_{12}$ and $\widehat{M}_{21}$ (Figure 3). We evaluated the
310 performance of our LSD implementation at identifying selected loci under these simulations
311 by plotting the true positive rate (TPR) against the false positive rate (FPR) under the choice

of HPDI thresholds from 0 to 1, and reporting the area under the curve (AUC) of the resultant receiver operating characteristic (ROC) curve (approximated by the Mann-Whitney U test (Delong & Carolina, 1988)). An AUC value of 0.5 reflects random assignment while that of 1 reflects perfect classification. To evaluate the accuracy of the inferred symmetry of the joint posterior (of reciprocal migration rates), we compared it to the true underlying selection coefficients, under the expectation that deviations from symmetry in the joint posterior should reflect asymmetry in selection regimes. Specifically, we determined for each locus l the posterior mass

$$\sigma_l = \int I\left(\frac{M_{21}}{M_{12}} < \frac{\widehat{M}_{21}}{\widehat{M}_{12}}\right)\pi_l(\theta)d_{\boldsymbol{\theta}},$$

where the indicator function $I(\cdot)$ limits the integral to cases in which the deviation of one of the migration rates has reduced more than the reciprocal migration rate compared to a proportional deviation of both migration rates from their neutral estimates $\widehat{M}_{12}$ and $\widehat{M}_{21}$. From this, we calculate the asymmetry as

$$a = \log\frac{\sigma}{1-\sigma},$$

where $\sigma = \frac{1}{n_s}\sum\sigma_l$ across loci simulated under selection.

AUC and asymmetry are reported for each simulated pseudo-genome, each representative of a unique demographic-selection regime.

ABC parametrization Migration rates were drawn from $log_{10}\, M_{12}, log_{10}\, M_{21} \sim U[-4,3]$ in all cases, while all other parameters were fixed to their true values ("fixed" parametrisation). We do this to assess the sensitivity and accuracy of LSD under ideal

conditions, and to not confound it with model and parameter misspecifications. For ABC parameter estimation, we retain the 1% closest simulations of 250,000 total simulations.

Comparison with other methods We compared the performance of LSD against that of two widely employed genome scan methods, on the simulated pseudo-genomes. pcadapt (Luu et al., 2017) identifies candidate SNPs as outliers with respect to population structure, ascertained via principal component analysis, while OutFLANK (Whitlock & Lotterhos, 2015) infers candidate SNPs by testing against a null model inferred from a highly revised Lewontin-Krakauer model extended to account for non-independent sampling of populations and sampling errors. Given that these approaches are SNP-based (whereas LSD is window-based), we consider a specific genomic window to be an outlier if at least one SNP within that window is called significant. This may reduce false negatives at the expense of inflating false positives, but reflects typical usage of such genome scans. For both methods, the true number of simulated populations was specified and SNPs were thinned to accommodate the particular LD structure of our simulated pseudo-genomes when computing PCs and calibrating the F_{ST} null distribution, before running on the full SNP dataset.

For a more realistic comparison where model parameters may not be known with confidence, we also considered cases of $\boldsymbol{\mathcal{M}_1}$ and $\boldsymbol{\mathcal{M}_4}$ in which all demographic parameters were unknown ("free" parametrisation) and drawn from large, uniform priors $log_{10}\, N_i \sim U[2,7],\ i = 1,2$ for $\boldsymbol{\mathcal{M}_1}$ and $log_{10}\, N_i \sim U[1.5,5],\ i = 1,\ldots,4$, $log_{10}\, T_{Dj} \sim U[-0.5,1],\ j = 1,2,3,\ log_{10}\alpha \sim U[0,1]$ and $log_{10}\, M_{adj} \sim U[0,1]$ for model $\boldsymbol{\mathcal{M}_4}$. Priors for M_{12}, M_{21} remained the same as before. We used the closest 10,000 out of 1,000,000 simulations to both

356 infer $\widehat{\boldsymbol{\theta}}$ and to identify outlier loci. For added realism, we inferred $\widehat{\boldsymbol{\theta}}$ from a full pseudo-
357 genome of 1,050 loci, of which 1,000 were neutral but 50 were mis-specified and weakly
358 selected with $s_{1,}\ s_2 = 0.001$; $T_S = 4{,}000$, $M_{12} = M_{21} = M$.
359

360 ## 2.4 Case study

361 To evaluate the performance of LSD on real data, we applied it to the detection of loci
362 underlying floral guides in two parapatric subspecies of *Antirrhinum majus*. *A.majus* is an
363 herbaceous, perennial, flowering plant native to the western Mediterranean. Owing to its
364 diploid inheritance, relatively short generation time, ability for both self- and cross-
365 pollination and rich and varied flower morphology, *A.majus* has lent itself as a model
366 organism for over a century, with several key floral genes being first identified within this
367 genus (Schwarz-Sommer, Davies, & Hudson, 2003; Schwinn et al., 2006). Two subspecies,
368 *A.m.striatum* and *A.m.pseudomajus,* differ in the flower colouration that signposts the
369 pollinator entry point, and form a natural hybrid zone in the Pyrenees that constitutes a
370 benchmark example of divergent selection (Whibley et al., 2006). Several genetic loci have
371 been shown to control the differences in these floral patterns (Bradley et al., 2017; Schwinn et
372 al., 2006), and recently, Tavares et al. (2018) produced evidence of genomic signatures of
373 selection at the ROS and EL loci, of which the former was functionally validated. Here, we
374 apply LSD to sequencing data from this study to isolate the ROS and EL loci and to
375 characterise their underlying selection signal. We filtered the data as in the original study, but
376 mapped on a more recent version of the *A.majus* reference (version 3.0; M. Li et al., 2019).
377

We modelled this study system via a simple representation (model $\boldsymbol{\mathcal{M}_1}$) of one population on either side of the hybrid zone (YP1 (*A.m.striatum*) vs MP2 (*A.m.pseudomajus*); populations 2.5km apart) and via a more inclusive island-continent model (model $\boldsymbol{\mathcal{M}_2}$) comprising three (distant) populations each per subspecies (CAM, ML, YP1 (*A.m.striatum*) vs MP2, CHI, CIN (*A.m.pseudomajus*); Figure S4), using an estimate of $\mu = 1.7 \times 10^{-8}$per bp per generation (Tavares et al., 2018) and allowing all N and M parameters to be free with priors $log_{10}\, N_j \sim U[1,7],\ j = 1,2, log_{10}M_{12}, log_{10}M_{21} \sim U[-4,4]$ for $\boldsymbol{\mathcal{M}_1}$ and $log_{10}N_j \sim U[3,7]$, $j = 1,2, log_{10}N_{ik} \sim U[1,6], k = 1,\ldots,6, log_{10}\, M_{12}, log_{10}M_{21} \sim U[-4,4]$ and $log_{10}M_{ic} \sim U[0,5]$ for $\boldsymbol{\mathcal{M}_2}$. In line with the available pool-seq data for this study, we simulated pooling of individuals in-silico by pooling twice the amount of msms coalescent (haploid) samples as (diploid) individuals in the pooled populations via *LSD-High*. Samples were drawn from a parametric (negative binomial) distribution fitted to the empirical coverage distribution using the '*fitdistrplus*' package (Delignette-Muller & Dutang, 2015) and *LSD-High*. We focused our analysis on chromosome 6 on which the ROS and EL loci lie. To acquire empirical estimates of neutral demographic parameters, we excluded all genomic regions present in the structural annotation plus 10kb flanking regions to generate a subset of putatively neutral regions on that chromosome. $\widehat{M}_{12}$ and $\widehat{M}_{21}$ were then estimated via 10kb windows from these neutral regions by retaining the closest 10,000 out of 1,000,000 simulations, as outlined above. To identify selected loci in the second step, we used sliding windows of size 10kb and a 1kb step-size, and retained the closest 5,000 out of the same 1,000,000 simulations.

3 RESULTS

3.1 Two-deme IM case (model $\boldsymbol{\mathcal{M}_1}$)

401 **Power to identify selected loci** While our LSD implementation exhibited conservative
402 p_l values (Figure S5), it demonstrated a high diagnostic ability to discriminate between
403 neutral and selected loci (AUC > 0.8) across a large range of migration-selection regimes
404 (Figure 5). Notably, our results point towards an optimal, intermediate rate of migration
405 ($M = 5$) at which selection is best detectable with high AUC values across a large set of
406 selection coefficients. As migration rates increase ($M = 50$), migration from the foreign deme
407 where selection acts on the alternate allele increasingly inhibits the build-up of beneficial
408 polymorphisms in the local deme, in which case the power to detect selected loci becomes
409 limited to scenarios under longer regimes of strong selection. At lower migration rates ($M =$
410 0.5), long regimes of selection permit the detection of loci under the lowest selection
411 coefficients, but power decreases for younger times compared to scenarios simulated under
412 intermediate migration rates. This owes to LSD relying on the reduction of effective
413 migration relative to neutral or genome-wide expectations, which in this case is already at a
414 low level.
415
416 The power to detect selection increased with increasing selection coefficients when
417 these were similar ($s_1 \approx s_2$, cells along diagonal of sub-panels in Figure 5). In such cases,
418 stronger selection coefficients on alternate alleles increasingly polarise and ultimately maintain
419 larger allele frequency differences between the two environments. In tandem, the power to
420 detect selection also generally increased with the time since the onset of selection T_S. In
421 contrast, when $s_1 \gg s_2$ or $s_1 \ll s_2$, one of the two alleles may proceed to fixation, in which
422 case the power to detect selection decays or is lost (e.g. grey cells in left-most column of sub-
423 panels when derived allele *A* is lost, and AUC values and inferred (a)symmetries tending

toward 0.5 and 0 respectively in bottom row cells when ancestral allele *a* is lost; Figure 5). This is particularly evident when the onset of selection is more distant in the past.

Power to characterise (a)symmetry A benefit of LSD over classic outlier approaches is that it can provide insight into genetic trade-offs underlying local adaptation, by identifying cases in which selection acts at equal strength in the two demes or metapopulations (symmetric AP), or whether selection coefficients differ considerably (CN or asymmetric AP). As shown in Figure 6, the inferred (a)symmetry generally reflected the true (a)symmetry of the underlying selection coefficients well, particularly for regimes with high power to correctly identify selected loci (Figure 5). In lower powered regimes, we observe some cases where the inferred asymmetry does not reflect the underlying asymmetry of the selection coefficients accurately (e.g. blue cells along diagonals in sub-panels at T_S = 4,000; Figures 6 and S6B). We interpret these results further in the discussion.

Standing variation vs *de-novo* A lower initial frequency of the derived allele may be expected to affect LSD's power to identify selected loci and its power to capture the underlying (a)symmetry of selection coefficients. However, we find that results for simulations building on selection from the *de-novo* and standing variation cases showed generally very similar patterns (Figures 5, 6 and S6). One notable exception however was the inaccurate inference of (a)symmetry in a few regimes with high power (AUC > 0.8) in the *de-novo* case (e.g. blue cells along diagonals in sub-panels at $T_S = 4{,}000$ in Figure S6B). This we attribute to the lower initial frequency of the derived allele *A* and consequently longer time needed to

approach drift-migration-selection equilibrium for the *de-novo* cases. This is explored further in the discussion.

3.2 More complex cases (models $\mathcal{M}_2$, $\mathcal{M}_3$ and $\mathcal{M}_4$)

A key feature of LSD is its potential to explicitly accommodate complex demographies, which can lead to an inflation in false positives when not properly accounted for (De Villemereuil, Frichot, Bazin, François, & Gaggiotti, 2014; Foll & Gaggiotti, 2008; Lotterhos & Whitlock, 2014). Despite the added complexity of models $\mathcal{M}_2$ and $\mathcal{M}_3$, results were generally very similar to that of model $\mathcal{M}_1$, with high power to identify selected loci (AUC > 0.8) across a large range of migration-selection regimes, an optimal migration rate at an intermediate value ($M = 5$), a similar dependence of power to detect selection on s_1, s_2 and T_S, and inferences of (a)symmetry that reflected well the underlying (a)symmetry of selection coefficients (Figures 7, S7 and S8). One notable difference between these models was that model $\mathcal{M}_2$ generally required longer time to generate power to detect selection when compared to models $\mathcal{M}_1$, $\mathcal{M}_3$ and $\mathcal{M}_4$, which we attribute to the larger meta-population N_E in model $\mathcal{M}_2$. For model $\mathcal{M}_4$, selection coefficients needed to be slightly higher ($s_1, s_2 \geq 0.01$; Figure S8) to attain high power to identify selected loci, and to accurately identify asymmetry.

3.3 Robustness to mis-specification of the neutral set

As shown for all models and a subset of the regimes ($M = 5$; $T_S = 40{,}000$; $s_1 = s_2 = 0.01, 0.1$), LSD is highly robust to the inclusion of selected loci in the neutral set, with

negligible reduction in power (AUC) at up to a 13% mis-specification for model $\boldsymbol{\mathcal{M}_4}$ and up to 20% for models $\boldsymbol{\mathcal{M}_1}$, $\boldsymbol{\mathcal{M}_2}$ and $\boldsymbol{\mathcal{M}_3}$ (Supplementary Text S5, Figure 4).

3.4 Comparison to other methods

The performance of LSD is comparable to that of pcadapt and OutFLANK under model $\boldsymbol{\mathcal{M}_1}$, with minimal difference between the methods across the range of migration-selection regimes (Figures 8 and S9). For the complex model $\boldsymbol{\mathcal{M}_4}$ however, both pcadapt and OutFLANK have little to no power to correctly identify selected loci (AUCs ~ 0.5; Figures 8 and S10), while LSD exhibits high AUC scores (> 0.8) in similar migration-selection regimes as it does under models $\boldsymbol{\mathcal{M}_1}$, $\boldsymbol{\mathcal{M}_2}$ and $\boldsymbol{\mathcal{M}_3}$. Importantly, the power of LSD to identify loci under selection was very similar (Figures 5, 8, S8A, S9A and S10A) when fixing $\widehat{M}_{12}$ and $\widehat{M}_{21}$ and all demographic parameters not affected by selection to their true value ("fixed" parametrisation), as when estimating $\widehat{M}_{12}$ and $\widehat{M}_{21}$ (Figures S11 and S12) and keeping all other parameters free ("free" parametrisation), implying that LSD is robust to parameter specification.

3.5 Case study results

We identified a region of reduced effective migration between 52.9-53.2MB on chromosome 6 (Figure 9), consistent with the location of the ROS and EL loci (Tavares et al., 2018). Under model $\boldsymbol{\mathcal{M}_1}$, this region is characterised by a set of smaller, multiple peaks (p_l < 0.01) reflecting signatures identified by previous authors, with the left-most peaks corresponding to ROS1 and ROS2 (shaded in red) and the right peaks to EL (shaded in green; Figure 9B). The joint posterior probability distributions reveal symmetric selection

acting on both regions, implying that selection acts with similar strength in the two populations. Under Model $\boldsymbol{\mathcal{M}_2}$, we find fewer outliers in the ROS-EL region than in model $\boldsymbol{\mathcal{M}_1}$, with the left-most peak in this region corresponding to ROS2 and the right peaks consistent with EL. ROS1 appears to be less of an outlier than in model $\boldsymbol{\mathcal{M}_1}$ ($p_l \approx 0.02$). In contrast to model $\boldsymbol{\mathcal{M}_1}$, the ROS2 and EL peaks in model $\boldsymbol{\mathcal{M}_2}$ are characterised by asymmetry, specifically with stronger selection acting in the populations of *A.m.pseudomajus* than in the populations of *A.m.striatum*.

4 DISCUSSION

The trajectory of selected loci depends on demographic and selection parameters that define the system, namely the effective population sizes, effective migration rates and selection coefficients, as well as the intrinsic properties of mutation and recombination. Despite well-developed theory which relates the effect of population parameters on the trajectory of selected alleles, few methods or empirical studies have combined estimates of differential selection with explicit quantification of migration rates and effective population sizes to examine the conditions under which local adaptation can arise. Here, we introduce such a method, LSD, which identifies candidate loci based on divergent population parameters using explicit demographic models, and demonstrate that under certain demographic-selection regimes, it can both detect and elucidate the processes underlying signatures of selection. While LSD is flexible regarding the choice of demographic models employed and can apply to single and multiple populations, we focus here specifically on processes that lead to selection against gene flow, namely local adaptation and extrinsic reproductive barriers, that can be inferred via their expectation to reduce M_E.

514

515 ## 4.1 Identifying selection

516 Using simulations, we demonstrate that LSD has high diagnostic power (AUC > 0.8)
517 to identify selected loci across a large range of demographic-selection regimes. This power
518 relies upon two fundamental aspects that contribute to generating observable patterns. First,
519 selection must effectively be realised, i.e. result in a frequency shift of the beneficial allele.
520 This requires that the strength of selection and initial frequency of the beneficial allele be
521 sufficient to both counter the homogenising effect of migration (Felsenstein, 1976; Haldane,
522 1930; Lenormand, 2002; Olson-Manning, Wagner, & Mitchell-Olds, 2012; M. Slatkin,
523 1973; Yeaman, 2015) and the eroding effect of drift (Wright, 1931). Secondly, the genomic
524 data must contain signatures of selection that can be detected. In the case of LSD, this
525 requires that the signatures of selection are discernible from the underlying noise (drift and
526 migration) that characterises the system, which demands sufficient time for said signatures to
527 be reflected in the employed statistics and hence in the inferred parameters N_E or M_E. A lack
528 of power in LSD must be interpreted considering these two conceptually different
529 perspectives. Notably, the lack of discrimination power for high migration rates and low
530 selection coefficients can be attributed to selection failing to realise as a consequence of local,
531 beneficial alleles being swamped by immigrant, maladaptive alleles. In contrast, the lack of
532 signal under low migration rates constitutes a methodological limitation of our implemented
533 model, as it becomes increasingly difficult to detect reductions in effective migration when
534 neutral or genome-wide migration rates are already at a low level; even when selection is
535 effectively being realised in the demes. This is analogous in effect to the loss of power to
536 detect selection in highly differentiated populations in F_{ST} outlier tests (Hoban et al., 2016;

537 Martin et al., 2013). Under the same principle, we argue that the converse expectation can be
538 assumed to hold for loci underlying adaptive introgression or balancing selection. That is, we
539 expect power to detect such loci to be low when populations are minimally differentiated and
540 high in highly divergent systems, as the detection of candidate loci in these cases is informed
541 by increased effective migration.
542
543 The power of LSD to correctly identify selected loci generally increases with stronger
544 selection coefficients and longer time since the onset of selection, though with exceptions.
545 Specifically, if selection is of similar or equal strength in both demes or meta-populations, we
546 observe a strong correlation between the power to detect selection and the true underlying
547 selection coefficients. This follows theory which states that the reduction in effective
548 migration is proportional to the strength of selection (Petry, 1983). However, we defer from
549 translating these changes to explicit selection coefficients because in addition to the strength
550 of selection, changes in effective migration are also a function of the recombination rate
551 between linked and selected loci (Cutter & Payseur, 2013; Lotterhos, 2019; Petry, 1983). If
552 selection differs strongly between demes or meta-populations ($s_i \gg s_j$), or when the onset of
553 selection is sufficiently distant in the past, however, one allele may become fixed in the
554 system. In such a case, the signal to detect selection rapidly decays (Huber, DeGiorgio,
555 Hellmann, & Nielsen, 2016; Przeworski, 2002). Moreover, we observed little power to detect
556 very recent selection, intrinsically related to our choice of summary statistics (Hohenlohe,
557 Phillips, & Cresko, 2010). That said, extending LSD to include additional statistics sensitive
558 to linkage disequilibrium such as extended haplotype homozygosity (EHH) (Sabeti et al.,
559 2002) or single density score (SDS) (Field et al., 2016) will increase the power to detect more

recent selection. Finally, given that LSD relies on localised deviations in effective demographic parameters, we predict that it may miss signals of polygenic selection, as signals of selection become increasingly hard to distinguish from the genomic background the smaller the locus effect sizes are.

From our simulations, we find that the power to detect selection is similar between the *de-novo* and standing genetic variation regimes (model $\mathcal{M}_1$; Figures 5 and S6A), likely as a result of only considering loci for which the derived allele was not lost. This particularly affected the *de-novo* case, under which the derived allele was lost in most simulations. Indeed, this is in line with theoretical expectation (Olson-Manning et al., 2012) and supports the notion that most empirical cases of local adaptation attribute selection of advantageous alleles to arise from standing variation (Jones et al., 2012; Lai et al., 2019; Reid et al., 2016). To clearly distinguish between these regimes, additional information on the evolutionary history of the system such as allele age, mutation rate or supplementary phylogenetic information is required (Peter et al., 2012).

4.2 Comparison to existing methods

LSD's power to detect selection is comparable with that of pcadapt and OutFLANK under the simple model $\mathcal{M}_1$, but strongly outperform these alternatives under the more complex model $\mathcal{M}_4$. These results appear to hold regardless of whether prior knowledge of model parameters is confidently known for LSD, as LSD exhibits similar performance under the ideal "fixed" and realistic "free" parametrisations. This suggests that the methods pcadapt and OutFLANK utilise to address population structure, namely PCA and an implicitly

583 modelled F_{ST} null distribution, respectively, are sufficient to control for the effects of relatively
584 simple demography, but insufficient to capture more complex demographies. By modelling
585 complex demographies explicitly, LSD is less affected by model complexity, though this extra
586 power comes with some costs.
587
588 Firstly, a demographic model needs to be specified that appropriately describes the
589 neutral genetic variation of the system, allows for inferences of selection through changes in
590 demographic parameters (e.g. $\boldsymbol{N}_E$ or $\boldsymbol{M}_E$), and is sufficiently simple to remain computationally
591 tractable. A preliminary analysis of model choice may therefore constitute a prerequisite to
592 successfully recapitulate the signal of complex evolutionary histories in the simulated data.
593 Importantly, the model should always be validated by demonstrating that the observed data
594 can be accurately and sufficiently captured (Figure S13).
595
596 Secondly, LSD remains computationally more demanding than both pcadapt and
597 OutFLANK. Inferring demographic parameters is generally computationally challenging as
598 the underlying genealogies need to be integrated out numerically (Hey & Nielsen, 2007),
599 which for complex models usually requires simulation-based approaches such as ABC.
600 Existing ABC approaches to infer locus-specific parameters (Bazin et al., 2010; Kousathanas
601 et al., 2016) are difficult to scale-up to genome-wide data as they require the simulation of
602 very many loci. To circumvent this problem, LSD implements an efficient ABC approach
603 that requires simulations of single loci only, which is possible because LSD neither attempts
604 to infer the hierarchical distribution of locus-specific parameters nor to obtain posterior
605 estimates on whether a locus is affected by selection. Instead, LSD identifies loci under

606 selection by quantifying whether locus-specific estimates of demographic parameters are
607 incompatible with those estimated from a set of putatively neutral loci.
608
609 The *a priori* identification of this neutral set constitutes the third requirement. Such a
610 set may be informed by the particular structural or functional class the sites belong to
611 (Williamson et al., 2005) and may for instance consist of genomic regions not linked to
612 structural annotations. Alternatively, a more naïve strategy may rely on the whole genome or a
613 random subset of the genome to reflect neutral diversity. Even if this assumption of neutrality
614 is violated (Begun et al., 2007; Fay, Wyckoff, & Wu, 2002; H. Li & Stephan, 2006), we
615 show that our method to estimate $\hat{\theta}$ is robust to the mis-identification of neutral loci, with
616 minimal effect on power even at high percentages of up to 20% mis-specification. We
617 attribute this to our method of estimating $\hat{\theta}$ as the product of per-locus posterior densities,
618 which amplifies the signal (density) according to majority rule.
619
620 We finally note that most widely applied genome scans methods (e.g. pcadapt and
621 OutFLANK) detect outliers at the SNP level, while our current implementation of LSD
622 focuses on genomic windows. Focusing on genomic windows offers a means to aggregate
623 information across linked loci, thereby potentially increasing power and reducing false
624 positives from spurious signals at individual SNPs (e.g. Galimberti et al., 2020). These
625 benefits are conditional on a choice of window size compatible with the LD decay in the
626 system, as this maximises the power and accuracy to capture the signal generated by selection.
627 The LSD framework is by no means limited to genomic windows however, and can be
628 extended to SNP data when using an appropriate simulator and summary statistics calculator.

629

630 ## 4.3 Revealing trade-offs underlying selection

631 LSD can also shed light on the directionality of selection by inferring the (a)symmetry
632 in deviations of migration rates between populations. In our simulations, this inferred
633 (a)symmetry accurately reflects the (a)symmetry in the underlying selection coefficients for
634 older onsets of selection, but less so for more recent onsets (Figures 6, 7B, S6B, S7B). This is
635 because inferred asymmetries in deviations of effective migration rates are also affected by
636 asymmetries in allele frequencies of the beneficial allele. For instance, a new beneficial
637 mutation that arises in one of two demes will initially be rare among migrants. Only as its
638 frequency increases will selection start to act against immigrants in both demes (Figure 10).
639 Hence, the inference of asymmetry in LSD may include cases where selection is effectively
640 asymmetric, but also those in which selection is effectively symmetric but prior to drift-
641 migration-selection equilibrium. A direct link between the inferred (a)symmetry in deviations
642 of migration rates and the (a)symmetry in underlying selection coefficients is only established
643 through time. We note that in practice, however, the interpretation of the results is
644 straightforward, as the inference of directionality is only meaningful for loci identified as
645 under selection i.e. with low p_l values. Such loci can only be inferred in regimes with high
646 AUC, which generally preclude regimes characterised by recent onsets of selection. For these
647 (high AUC) regimes, we generally find the estimated (a)symmetries to reflect the true
648 (a)symmetry in selection coefficients accurately. Stated succinctly, LSD's inferred
649 directionality is generally accurate and meaningful for identified candidates, and potentially
650 inaccurate but irrelevant for other loci.

651

652 The ability of LSD to infer the directionality of selection directly from genomic data
653 can greatly facilitate investigations of genetic trade-offs underlying adaptation, which are
654 seldom performed due to the considerable effort required to set up field trials of recombinant
655 lines. As shown above, the inference of symmetry in LSD-identified candidates accurately
656 reflects cases of AP with equal strength of selection on alternate alleles in the contrasting
657 environments. The inference of asymmetry on the other hand can either indicate AP with
658 stronger selection in one environment than the other, or CN. From our simulations, we find
659 that scenarios reflecting AP are generally more readily detected than those reflecting CN.
660 Given that selection acts only upon one of the two alleles in the latter case, fixation becomes
661 likely and the ability to detect selection is transient. This implies that there may be an
662 observation bias between AP and CN; such that the inference of CN may be comparatively
663 under-represented. This bias appears to contrast with that reported in ecological literature,
664 where instances of AP are more rarely detected compared to CN due to the additional power
665 required to statistically prove differential fitness concurrently in two environments (Anderson
666 et al., 2013). LSD may further complement field trials as such experiments typically test
667 genetic trade-offs under contemporary selective environments, which may not reflect past
668 conditions driving the observed adaptive responses, but whose signature may still be inferred
669 from genomic data. Using LSD to formulate expectations about fitness effects and to inform
670 the choice of environmental conditions under which to validate identified candidate genes can
671 thus greatly aid such experiments.
672

673 **4.3 Real-world application**

674 We demonstrate a real-world application of LSD by successfully isolating and
675 characterising the selection signal of loci underlying an extrinsic reproductive barrier in
676 *A.majus*. Our results from contrasting a single population (model $\boldsymbol{\mathcal{M}_1}$) and three populations
677 (model $\boldsymbol{\mathcal{M}_2}$) per subspecies both identified the ROS and EL loci which were previously
678 reported to underlie differences in floral patterns between these subspecies (Tavares et al.,
679 2018). Interestingly however, our results characterise selection at these loci as symmetric
680 under model $\boldsymbol{\mathcal{M}_1}$ and asymmetric with stronger selection acting on *A.m.pseudomajus* than in
681 *A.m.striatum* under model $\boldsymbol{\mathcal{M}_2}$. This exemplifies that results of LSD genome scans are
682 conditional on the model and populations used, such that here, model $\boldsymbol{\mathcal{M}_1}$ uncovers
683 population-pair specific differences at the contact zone (YP1 vs MP2) while model $\boldsymbol{\mathcal{M}_2}$
684 reveals common (global) differences between the two subspecies. We do not necessarily expect
685 these two signals to be identical, and indeed, Tavares et al. (2018) showed different θ_W and
686 F_{ST} estimates between distant and close *A.m.striatum-A.m.pseudomajus* population pairs.
687 Given that there is no evident difference in environment or pollinators on opposite sides of
688 the hybrid zone, reproductive barriers in this system have often been proposed to be
689 maintained through selection against hybrids and frequency-dependent sexual selection
690 mediated by pollinator preference for the dominant flower phenotype on either side of the
691 contact zone. However, whether selection on alternate alleles follows the same positive
692 frequency-dependence across the broader scale including more distant populations is currently
693 unknown. The difference in signal between local pairs at the contact zone ($\boldsymbol{\mathcal{M}_1}$) and the
694 global set ($\boldsymbol{\mathcal{M}_2}$) may be generated by different frequency-dependent selection curves for the
695 alternate alleles and potentially loss of AP away from the contact zone (Figure S14).
696

697 # 5 CONCLUSION

698 Loci under selection are predicted to exhibit genealogies with demographic parameters
699 divergent from those of neutral non-linked regions, leading to heterogeneity in demography
700 across the genome. In this study, we condition the identification of candidate loci on
701 divergent population parameters using explicit demographic models, and demonstrate that
702 under certain conditions of migration, selection strength and onset time, we can both detect
703 and elucidate the underlying processes driving signatures of selection. Incorporating and
704 utilising the inference of demographic parameters in the identification of candidate loci
705 address some key issues and assumptions that prevail in the discrimination of selected
706 variants, namely 1) the explicit consideration of demography, 2) heterogeneity in drift and
707 gene flow across the genome, 3) information synthesis of multiple, complementary summary
708 statistics, and 4) transparency towards underlying driving mechanisms.
709

710 Our power analysis using simulations shows that LSD, and our implementation of it,
711 represents a powerful method for detecting selection that is robust to different and complex
712 demographies. Furthermore, given that certain demographic parameters, e.g. migration, are
713 not inherently commutative, we show that the directionality or population-specificity in
714 selection can be inferred. This can facilitate identifying in which environment selection acts
715 and hence elucidate genetic trade-offs; bridging an analytical divide between experimental
716 ecology and population genomics. Importantly, the proposed approach as well as our
717 implementation is not limited to the demographic models investigated here, nor the explicit
718 choice of simulation programs or summary statistics used. This flexibility and customisability
719 of LSD can facilitate e.g. more realistic accommodation of recombination (via different

720 coalescent simulators), improved detection of more recent selection (via linkage-informative
721 statistics), and inference of other modes of selection (e.g. balancing selection) and adaptive
722 introgression by conditioning the detection of selection on e.g. increase (rather than
723 reduction) of M_E or changes in N_E relative to neutral expectations.
724

725 ## ACKNOWLEDGEMENTS

726 We would like to thank the Genetic Diversity Centre at ETH Zurich and in
727 particular Niklaus Zemp for providing IT support. This work was supported by the Swiss
728 National Science Foundation (SNSF) grants 31003A_160123 and 31003A_182675 awarded
729 to AW and grant 31003A_173062 awarded to DW.
730

REFERENCES

Aeschbacher, S., Futschik, A., & Beaumont, M. A. (2013). Approximate Bayesian computation for modular inference problems with many parameters: The example of migration rates. *Molecular Ecology*, *22*(4), 987–1002. https://doi.org/10.1111/mec.12165

Anderson, J. T., Lee, C.-R., & Mitchell-Olds, T. (2014). Strong selection genome-wide enhances fitness tradeoffs across environments and episodes of selection, *68*(1), 16–31. https://doi.org/10.1111/evo.12259.Strong

Anderson, J. T., Lee, C. R., Rushworth, C., Colautti, R., & Mitchell-Olds, T. (2013). Genetic tradeoffs and conditional neutrality contribute to local adaptation. *Molecular Ecology*, *22*(3), 699–708. https://doi.org/10.1038/jid.2014.371

Balding, D. J., & Nichols, R. A. (1994). DNA profile match probability calculation: how to allow for population stratification, relatedness, database selection and single bands. *Forensic Science International*, *64*(2–3), 125–140. https://doi.org/10.1016/0379-0738(94)90222-4

Barton, N., & Bengtsson, B. O. (1986). The barrier to genetic exchange between hybridising populations. *Heredity*, *57*(3), 357–376. https://doi.org/10.1038/hdy.1986.135

Bazin, E., Dawson, K. J., & Beaumont, M. A. (2010). Likelihood-free inference of population structure and local adaptation in a Bayesian hierarchical model. *Genetics*, *185*(2), 587–602. https://doi.org/10.1534/genetics.109.112391

Beaumont, M. A., & Nichols, R. A. (1996). Evaluating loci for use in the genetic analysis of population structure. *Proceedings of the Royal Society B: Biological Sciences*, *263*(1377), 1619–1626. https://doi.org/10.1098/rspb.1996.0237

Beaumont, Mark A., & Balding, D. J. (2004). Identifying adaptive genetic divergence among populations from genome scans. *Molecular Ecology*, *13*(4), 969–980. https://doi.org/10.1111/j.1365-294X.2004.02125.x

Beaumont, Mark A., Zhang, W., & Balding, D. J. (2002). Approximate Bayesian computation in population genetics. *Genetics*, *162*(4), 2025–2035. https://doi.org/10.1111/j.1937-2817.2010.tb01236.x

Begun, D. J., Holloway, A. K., Stevens, K., Hillier, L. W., Poh, Y. P., Hahn, M. W., … Langley, C. H. (2007). Population genomics: Whole-genome analysis of polymorphism and divergence in Drosophila simulans. *PLoS Biology*, *5*(11), 2534–2559. https://doi.org/10.1371/journal.pbio.0050310

Bierne, N., Welch, J., Loire, E., Bonhomme, F., & David, P. (2011). The coupling hypothesis: Why genome scans may fail to map local adaptation genes. *Molecular Ecology*, *20*(10), 2044–2072. https://doi.org/10.1111/j.1365-294X.2011.05080.x

Biswas, S., & Akey, J. M. (2006). Genomic insights into positive selection. *Trends in Genetics*, *22*(8), 437–446. https://doi.org/10.1016/j.tig.2006.06.005

Bradley, D., Xu, P., Mohorianu, I. I., Whibley, A., Field, D., Tavares, H., … Coen, E. (2017). Evolution of flower color pattern through selection on regulatory small RNAs. *Science*, *358*(6365), 925–928. https://doi.org/10.1126/science.aao3526

Charlesworth, B. (2009). Fundamental concepts in genetics: Effective population size and patterns of molecular evolution and variation. *Nature Reviews Genetics*, *10*(3), 195–205. https://doi.org/10.1038/nrg2526

Charlesworth, B., Nordborg, M., & Charlesworth, D. (1997). The effects of background and

interference selection on patterns of genetic variation in subdivided populations. *Genetics Research*, *70*, 155–174. https://doi.org/10.1534/genetics.115.178558

Cutter, A. D., & Payseur, B. A. (2013). Genomic signatures of selection at linked sites: Unifying the disparity among species. *Nature Reviews Genetics*, *14*(4), 262–274. https://doi.org/10.1038/nrg3425

De Villemereuil, P., Frichot, É., Bazin, É., François, O., & Gaggiotti, O. E. (2014). Genome scan methods against more complex models: When and how much should we trust them? *Molecular Ecology*, *23*(8), 2006–2019. https://doi.org/10.1111/mec.12705

Delignette-Muller, M. L., & Dutang, C. (2015). fitdistrplus: An R package for fitting distributions. *Journal of Statistical Software*, *64*(4), 1–34. https://doi.org/10.18637/jss.v064.i04

Delong, E. R., & Carolina, N. (1988). Comparing the Areas under Two or More Correlated Receiver Operating Characteristic Curves : A Nonparametric Approach Author (s): Elizabeth R . DeLong , David M . DeLong and Daniel L . Clarke-Pearson Published by : International Biometric Society Stable. *Biometrics*, *44*(3), 837–845.

Dussex, N., Wegmann, D., & Robertson, B. C. (2014). Postglacial expansion and not human influence best explains the population structure in the endangered kea (Nestor notabilis). *Molecular Ecology*, *23*(9), 2193–2209. https://doi.org/10.1111/mec.12729

Edmonds, C. a, Lillie, A. S., & Cavalli-Sforza, L. L. (2004). Mutations arising in the wave front of an expanding population. *Proceedings of the National Academy of Sciences of the United States of America*, *101*(4), 975–979. https://doi.org/10.1073/pnas.0308064100

Ewing, G., & Hermisson, J. (2010). MSMS: A coalescent simulation program including recombination, demographic structure and selection at a single locus. *Bioinformatics*, *26*(16), 2064–2065. https://doi.org/10.1093/bioinformatics/btq322

Excoffier, L., Hofer, T., & Foll, M. (2009). Detecting loci under selection in a hierarchically structured population. *Heredity*, *103*(4), 285–298. https://doi.org/10.1038/hdy.2009.74

Excoffier, Laurent, Foll, M., & Petit, R. J. (2009). Genetic Consequences of Range Expansions. *Annual Review of Ecology, Evolution, and Systematics*, *40*(1), 481–501. https://doi.org/10.1146/annurev.ecolsys.39.110707.173414

Fay, J. C., Wyckoff, G. J., & Wu, C. I. (2002). Testing the neutral theory of molecular evolution with genomic data from Drosophila. *Nature*, *415*(6875), 1024–1026. https://doi.org/10.1038/4151024a

Felsenstein, J. (1976). The theoretical population genetics of variable selection and migration. *Annu. Rev. Genet*, *10*, 253–280.

Field, Y., Boyle, E. A., Telis, N., Gao, Z., Gaulton, K. J., Yengo, L., … Pritchard, J. K. (2016). Detection of human adaptation during the past 2000 years, *354*(6313), 760–764. https://doi.org/10.1126/science.aag0776.Detection

Foll, M., & Gaggiotti, O. (2008). A genome-scan method to identify selected loci appropriate for both dominant and codominant markers: A Bayesian perspective. *Genetics*, *180*(2), 977–993. https://doi.org/10.1534/genetics.108.092221

Foll, M., Gaggiotti, O. E., Daub, J. T., Vatsiou, A., & Excoffier, L. (2014). Widespread signals of convergent adaptation to high altitude in Asia and America. *American Journal of Human Genetics*, *95*(4), 394–407. https://doi.org/10.1016/j.ajhg.2014.09.002

Foll, M., Poh, Y. P., Renzette, N., Ferrer-Admetlla, A., Bank, C., Shim, H., … Jensen, J. D. (2014). Influenza Virus Drug Resistance: A Time-Sampled Population Genetics Perspective. *PLoS Genetics*, *10*(2). https://doi.org/10.1371/journal.pgen.1004185

François, O., Martins, H., Caye, K., & Schoville, S. D. (2016). Controlling false discoveries in genome scans for selection. *Molecular Ecology*, *25*(2), 454–469. https://doi.org/10.1111/mec.13513

Fusco, D., & Uyenoyama, M. K. (2011). Sex-specific incompatibility generates locus-specific rates of introgression between species. *Genetics*, *189*(1), 267–288. https://doi.org/10.1534/genetics.111.130732

Galimberti, M., Leuenberger, C., Wolf, B., Szilágyi, S. M., Foll, M., & Wegmann, D. (2020). Detecting selection from linked sites using an F-model. *Genetics*, *216*(4), 1205–1215. https://doi.org/10.1534/genetics.120.303780

Galtier, N., Depaulis, F., & Barton, N. H. (2000). Detecting bottlenecks and selective sweeps from DNA sequence polymorphism. *Genetics*, *155*(2), 981–987.

Geraldes, A., Ferrand, N., & Nachman, M. W. (2006). Contrasting patterns of introgression at X-linked loci across the hybrid zone between subspecies of the European rabbit (Oryctolagus cuniculus). *Genetics*, *173*(2), 919–933. https://doi.org/10.1534/genetics.105.054106

Gossmann, T. I., Woolfit, M., & Eyre-Walker, A. (2011). Quantifying the variation in the effective population size within a genome. *Genetics*, *189*(4), 1389–1402. https://doi.org/10.1534/genetics.111.132654

Haldane, J. B. S. (1930). A mathematical theory of natural and artificial selection. (Part VI, Isolation.). *Math. Proc. Cambridge Philos. Soc.*, *26*, 220–230.

Hey, J., & Nielsen, R. (2007). Integration within the Felsenstein equation for improved Markov chain Monte Carlo methods in population genetics. *Proceedings of the National Academy of Sciences of the United States of America*, *104*(8), 2785–2790. https://doi.org/10.1073/pnas.0611164104

Hoban, S., Kelley, J. L., Lotterhos, K. E., Antolin, M. F., Bradburd, G., Lowry, D. B., … Whitlock, M. C. (2016). Finding the genomic basis of local adaptation: Pitfalls, practical solutions, and future directions. *American Naturalist*, *188*(4), 379–397. https://doi.org/10.1086/688018

Hofer, T., Ray, N., Wegmann, D., & Excoffier, L. (2009). Large allele frequency differences between human continental groups are more likely to have occurred by drift during range expansions than by selection. *Annals of Human Genetics*, *73*(1), 95–108. https://doi.org/10.1111/j.1469-1809.2008.00489.x

Hohenlohe, P. A., Phillips, P. C., & Cresko, W. A. (2010). Using population genomics to detect selection in natural populations: Key concepts and methodological considerations. *International Journal of Plant Sciences*, *171*(9), 1059–1071. https://doi.org/10.1086/656306

Horscroft, C., Ennis, S., Pengelly, R. J., Sluckin, T. J., & Collins, A. (2019). Sequencing era methods for identifying signatures of selection in the genome. *Briefings in Bioinformatics*, *20*(6), 1997–2008. https://doi.org/10.1093/bib/bby064

Huber, C. D., DeGiorgio, M., Hellmann, I., & Nielsen, R. (2016). Detecting recent selective sweeps while controlling for mutation rate and background selection. *Molecular Ecology*, *25*(1), 142–156. https://doi.org/10.1111/mec.13351

Jones, F. C., Grabherr, M. G., Chan, Y. F., Russell, P., Mauceli, E., Johnson, J., … Kingsley, D. M. (2012). The genomic basis of adaptive evolution in threespine sticklebacks. *Nature*, *484*(7392), 55–61. https://doi.org/10.1038/nature10944

Joyce, P., & Marjoram, P. (2008). Approximately sufficient statistics and bayesian

computation. *Statistical Applications in Genetics and Molecular Biology*, *7*(1). https://doi.org/10.2202/1544-6115.1389

Kawecki, T. J., & Ebert, D. (2004). Conceptual issues in local adaptation. *Ecology Letters*, *7*(12), 1225–1241. https://doi.org/10.1111/j.1461-0248.2004.00684.x

Kingman, J. F. C. (1982). The coalescent. *Stochastic Processes and Their Applications*, *13*(3), 235–248. https://doi.org/10.1016/0304-4149(82)90011-4

Korneliussen, T. S., Albrechtsen, A., & Nielsen, R. (2014). ANGSD: Analysis of Next Generation Sequencing Data. *BMC Bioinformatics*, *15*(1), 356. https://doi.org/10.1186/s12859-014-0356-4

Kousathanas, A., Leuenberger, C., Helfer, J., Quinodoz, M., & Foll, M. (2016). Likelihood-free inference in high-dimensional models. *Genetics*, *203*(2), 893–904. https://doi.org/10.1534/genetics.116.187567

Lai, Y. T., Yeung, C. K. L., Omland, K. E., Pang, E. L., Hao, Y., Liao, B. Y., … Li, S. H. (2019). Standing genetic variation as the predominant source for adaptation of a songbird. *Proceedings of the National Academy of Sciences of the United States of America*, *116*(6), 2152–2157. https://doi.org/10.1073/pnas.1813597116

Lenormand, T. (2002). Gene flow and the limits to natural selection. *Trends in Ecology & Evolution*, *17*(4), 183–189. https://doi.org/10.1111/j.1365-2184.1976.tb01248.x

Li, H., & Stephan, W. (2006). Inferring the demographic history and rate of adaptive substitution in Drosophila. *PLoS Genetics*, *2*(10), 1580–1589. https://doi.org/10.1371/journal.pgen.0020166

Li, J., Li, H., Jakobsson, M., Li, S., SjÖdin, P., & Lascoux, M. (2012). Joint analysis of demography and selection in population genetics: Where do we stand and where could we go? *Molecular Ecology*, *21*(1), 28–44. https://doi.org/10.1111/j.1365-294X.2011.05308.x

Li, M., Zhang, D., Gao, Q., Luo, Y., Zhang, H., Ma, B., … Xue, Y. (2019). Genome structure and evolution of Antirrhinum majus L. *Nature Plants*, *5*(2), 174–183. https://doi.org/10.1038/s41477-018-0349-9

Lotterhos, K. E. (2019). The effect of neutral recombination variation on genome scans for selection. *G3: Genes, Genomes, Genetics*, *9*(6), 1851–1867. https://doi.org/10.1534/g3.119.400088

Lotterhos, K. E., & Whitlock, M. C. (2014). Evaluation of demographic history and neutral parameterization on the performance of FST outlier tests. *Molecular Ecology*, *23*(9), 2178–2192. https://doi.org/10.1111/mec.12725

Luikart, G., England, P. R., Tallmon, D., Jordan, S., & Taberlet, P. (2003). The power and promise of population genomics: From genotyping to genome typing. *Nature Reviews Genetics*, *4*(12), 981–994. https://doi.org/10.1038/nrg1226

Luu, K., Bazin, E., & Blum, M. G. B. (2017). pcadapt: an R package to perform genome scans for selection based on principal component analysis. *Molecular Ecology Resources*, *17*(1), 67–77. https://doi.org/10.1111/1755-0998.12592

Marjoram, P., & Tavaré, S. (2006). Modern computational approaches for analysing molecular genetic variation data. *Nature Reviews Genetics*, *7*(10), 759–770. https://doi.org/10.1038/nrg1961

Martin, S. H., Dasmahapatra, K. K., Nadeau, N. J., Salazar, C., Walters, J. R., Simpson, F., … Jiggins, C. D. (2013). Genome-wide evidence for speciation with gene flow in Heliconius butterflies. *Genome Research*, *23*(11), 1817–1828.

https://doi.org/10.1101/gr.159426.113
Naisbit, R. E., Jiggins, C. D., & Mallet, J. (2001). Disruptive sexual selection against hybrids contributes to speciation between Heliconius cydno and Heliconius melpomene. *Proceedings of the Royal Society B: Biological Sciences*, *268*(1478), 1849–1854. https://doi.org/10.1098/rspb.2001.1753
Nosil, P., Vines, T. H., & Funk, D. J. (2005). Perspective: Reproductive Isolation Caused By Natural Selection Against Immigrants From Divergent Habitats. *Evolution*, *59*(4), 705. https://doi.org/10.1554/04-428
Oakley, C. G., Ågren, J., Atchison, R. A., & Schemske, D. W. (2014). QTL mapping of freezing tolerance: Links to fitness and adaptive trade-offs. *Molecular Ecology*, *23*(17), 4304–4315. https://doi.org/10.1111/mec.12862
Oleksyk, T. K., Smith, M. W., & O'Brien, S. J. (2010). Genome-wide scans for footprints of natural selection. *Philosophical Transactions of the Royal Society B: Biological Sciences*, *365*(1537), 185–205. https://doi.org/10.1098/rstb.2009.0219
Olson-Manning, C. F., Wagner, M. R., & Mitchell-Olds, T. (2012). Adaptive evolution: Evaluating empirical support for theoretical predictions. *Nature Reviews Genetics*, *13*(12), 867–877. https://doi.org/10.1038/nrg3322
Peter, B. M., Huerta-Sanchez, E., & Nielsen, R. (2012). Distinguishing between Selective Sweeps from Standing Variation and from a De Novo Mutation. *PLoS Genetics*, *8*(10). https://doi.org/10.1371/journal.pgen.1003011
Petry, D. (1983). The effect on neutral gene flow of selection at a linked locus. *Theoretical Population Biology*, *23*(3), 300–313. https://doi.org/10.1016/0040-5809(83)90020-5
Przeworski, M. (2002). The Signature of Positive Selection at Randomly Chosen Loci. *Genetics*, *162*(4), 1179–1189.
Rannala, B., & Hartigan, J. A. (1996). Estimating gene flow in island populations. *Genetical Research*, *67*(2), 147–158. https://doi.org/10.1017/s0016672300033607
Reid, N. M., Proestou, D. A., Clark, B. W., Warren, W. C., Colbourne, J. K., Shaw, J. R., … Whitehead, A. (2016). The genomic landscape of rapid repeated evolutionary adaptation to toxic pollution in wild fish. *Science*, *354*(6317), 1305–1308. https://doi.org/10.1126/science.aah4993
Rundle, H. D., & Whitlock, M. C. (2001). A genetic interpretation of ecologically dependent isolation. *Evolution*, *55*(1), 198–201.
Sabeti, P. C., Reich, D. E., Higgins, J. M., Levine, H. Z. P., Richter, D. J., Schaffner, S. F., … Lander, E. S. (2002). Detecting recent positive selection in the human genome from haplotype structure. *Nature*, *419*(6909), 832–837. https://doi.org/10.1038/nature01140
Savolainen, O., Lascoux, M., & Merilä, J. (2013). Ecological genomics of local adaptation. *Nature Reviews Genetics*, *14*(11), 807–820. https://doi.org/10.1038/nrg3522
Schluter, D. (2000). *The Ecology of Adaptive Radiation*. Oxford University Press, Oxford, U.K. Retrieved from https://global.oup.com/academic/product/the-ecology-of-adaptive-radiation-9780198505228?cc=ch&lang=en&
Schwarz-Sommer, Z., Davies, B., & Hudson, A. (2003). An everlasting pioneer: The story of Antirrhinum research. *Nature Reviews Genetics*, *4*(8), 655–664. https://doi.org/10.1038/nrg1127
Schwinn, K., Venail, J., Shang, Y., Mackay, S., Alm, V., Butelli, E., … Martin, C. (2006). A Small Family of MYB-Regulatory Genes Controls Floral Pigmentation Intensity and Patterning in the Genus Antirrhinum. *The Plant Cell*, *18*(April), 831–851.

https://doi.org/10.1105/tpc.105.039255.1
Sisson, S., Fan, Y., & Beaumont, M. (2018). *Handbook of Approximate Bayesian Computation*. (S. Sisson, Y. Fan, & M. Beaumont, Eds.) (1st ed.). Boca Raton: Chapman and Hall/CRC. https://doi.org/https://doi.org/10.1201/9781315117195
Slatkin, M. (1973). Gene flow and selection in a cline. *Genetics*, *75*(4), 733–756.
Slatkin, Montgomery, & Excoffier, L. (2012). Serial founder effects during range expansion: A spatial analog of genetic drift. *Genetics*, *191*(1), 171–181. https://doi.org/10.1534/genetics.112.139022
Sousa, V. C., Carneiro, M., Ferrand, N., & Hey, J. (2013). Identifying loci under selection against gene flow in isolation-with-migration models. *Genetics*, *194*(1), 211–233. https://doi.org/10.1534/genetics.113.149211
Tavaré, S., Balding, D. J., Griffiths, R. C., & Donnelly, P. (1997). Inferring coalescence times from DNA sequence data. *Genetics*, *145*(2), 505–518.
Tavares, H., Whibley, A., Field, D. L., Bradley, D., Couchman, M., & Copsey, L. (2018). Selection and gene flow shape genomic islands that control floral guides, 1–6. https://doi.org/10.1073/pnas.1801832115
Thalmann, O., Wegmann, D., Spitzner, M., Arandjelovic, M., Guschanski, K., Leuenberger, C., … Vigilant, L. (2011). Historical sampling reveals dramatic demographic changes in western gorilla populations. *BMC Evolutionary Biology*, *11*(1). https://doi.org/10.1186/1471-2148-11-85
Troth, A., Puzey, J. R., Kim, R. S., Willis, J. H., & Kelly, J. K. (2018). Selective trade-offs maintain alleles underpinning complex trait variation in plants, *478*(August), 475–478.
Vitti, J. J., Grossman, S. R., & Sabeti, P. C. (2013). Detecting Natural Selection in Genomic Data. *Annual Review of Genetics*, *47*(1), 97–120. https://doi.org/10.1146/annurev-genet-111212-133526
Wakeley, J. (2001). The coalescent in an island model of population subdivision with variation among demes. *Theoretical Population Biology*, *59*(2), 133–144. https://doi.org/10.1006/tpbi.2000.1495
Wegmann, D., & Excoffier, L. (2010). Bayesian inference of the demographic history of chimpanzees. *Molecular Biology and Evolution*, *27*(6), 1425–1435. https://doi.org/10.1093/molbev/msq028
Wegmann, D., Leuenberger, C., & Excoffier, L. (2009). Efficient approximate Bayesian computation coupled with Markov chain Monte Carlo without likelihood. *Genetics*, *182*(4), 1207–1218. https://doi.org/10.1534/genetics.109.102509
Wegmann, D., Leuenberger, C., Neuenschwander, S., & Excoffier, L. (2010). ABCtoolbox: a versatile toolkit for approximate Bayesian computations. *BMC Bioinformatics*, *11*, 116. https://doi.org/10.1186/1471-2105-11-116
Whibley, A. C., Langlade, N. B., Andalo, C., Hanna, A. I., Bangham, A., Thébaud, C., & Coen, E. (2006). Evolutionary paths underlying flower color variation in Antirrhinum. *Science*, *313*(5789), 963–966. https://doi.org/10.1126/science.1129161
Whitlock, M. C., & Lotterhos, K. E. (2015). Reliable detection of loci responsible for local adaptation: Inference of a null model through trimming the distribution of FST. *American Naturalist*, *186*(October), S24–S36. https://doi.org/10.1086/682949
Williamson, S. H., Hernandez, R., Fledel-alon, A., Zhu, L., Nielsen, R., & Bustamante, C. D. (2005). Simultaneous inference of selection and population growth from patterns of variation in the human genome. *PNAS*, *102*(22), 7882–7887. Retrieved from

http://www.pubmedcentral.nih.gov/articlerender.fcgi?artid=1142382&tool=pmcentrez&rendertype=abstract
Won, Y. J., Sivasundar, A., Wang, Y., & Hey, J. (2005). On the origin of Lake Malawi cichlid species: A population genetic analysis of divergen. *Systematics and the Origin of Species: On Ernst Mayr's 100th Anniversary*, *102*, 182–200. https://doi.org/10.17226/11310
Wright, S. (1931). Evolution in Mendelian Populations. *Genetics*, *16*(2), 97–159.
Yeaman, S. (2015). Local adaptation by alleles of small effect. *American Naturalist*, *186*, S74–S89. https://doi.org/10.1086/682405

DATA ACCESSIBILITY

We provide scripts to perform LSD genome scans at the GitHub repository: https://github.com/hirzi/LSD.

AUTHOR CONTRIBUTIONS

HL, DW, AW and SF designed the study. HL wrote the LSD scripts and performed the simulations and analyses. HL and DW developed the methods. HL wrote the manuscript, which all authors critically revised.

FIGURES

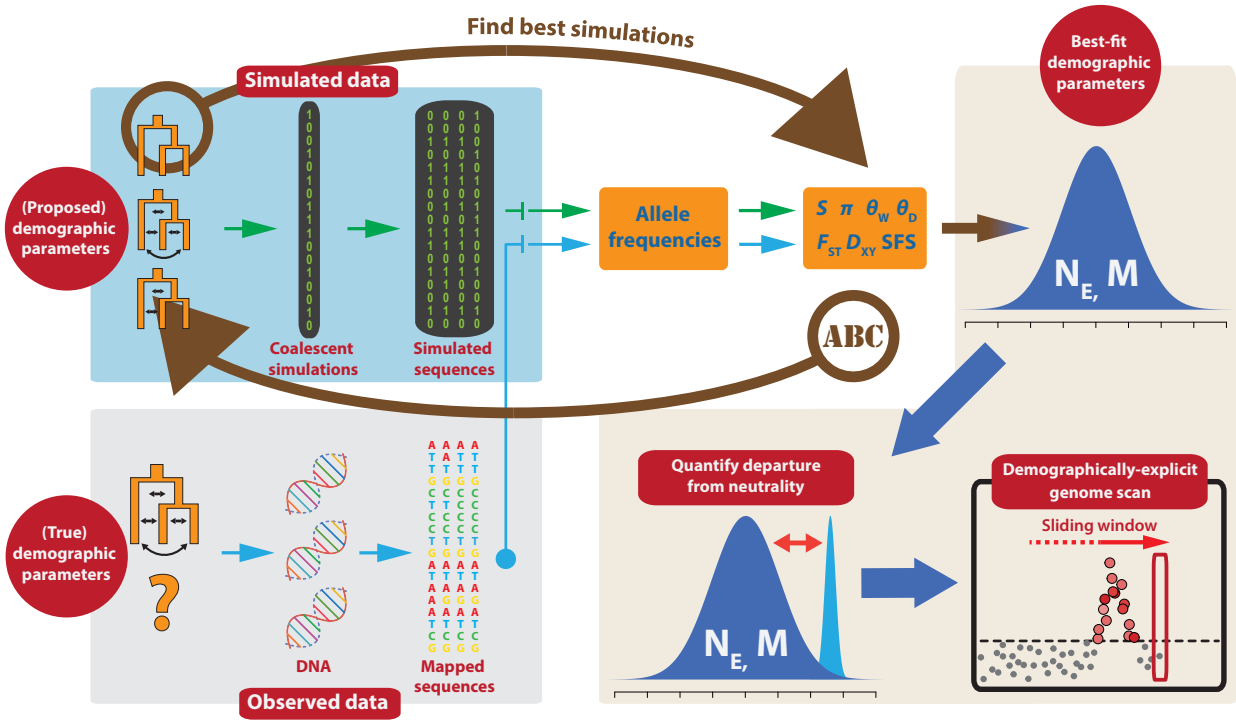

Figure 1. Analytical framework to identify Loci under Selection via explicit Demographic models (LSD). LSD identifies loci under selection by first estimating demographic parameters and then quantifying the departure of these parameters from neutral expectations. Our specific implementation of LSD employs Approximate Bayesian Computation (ABC) for parameter estimation, and is performed in a genome scan approach.

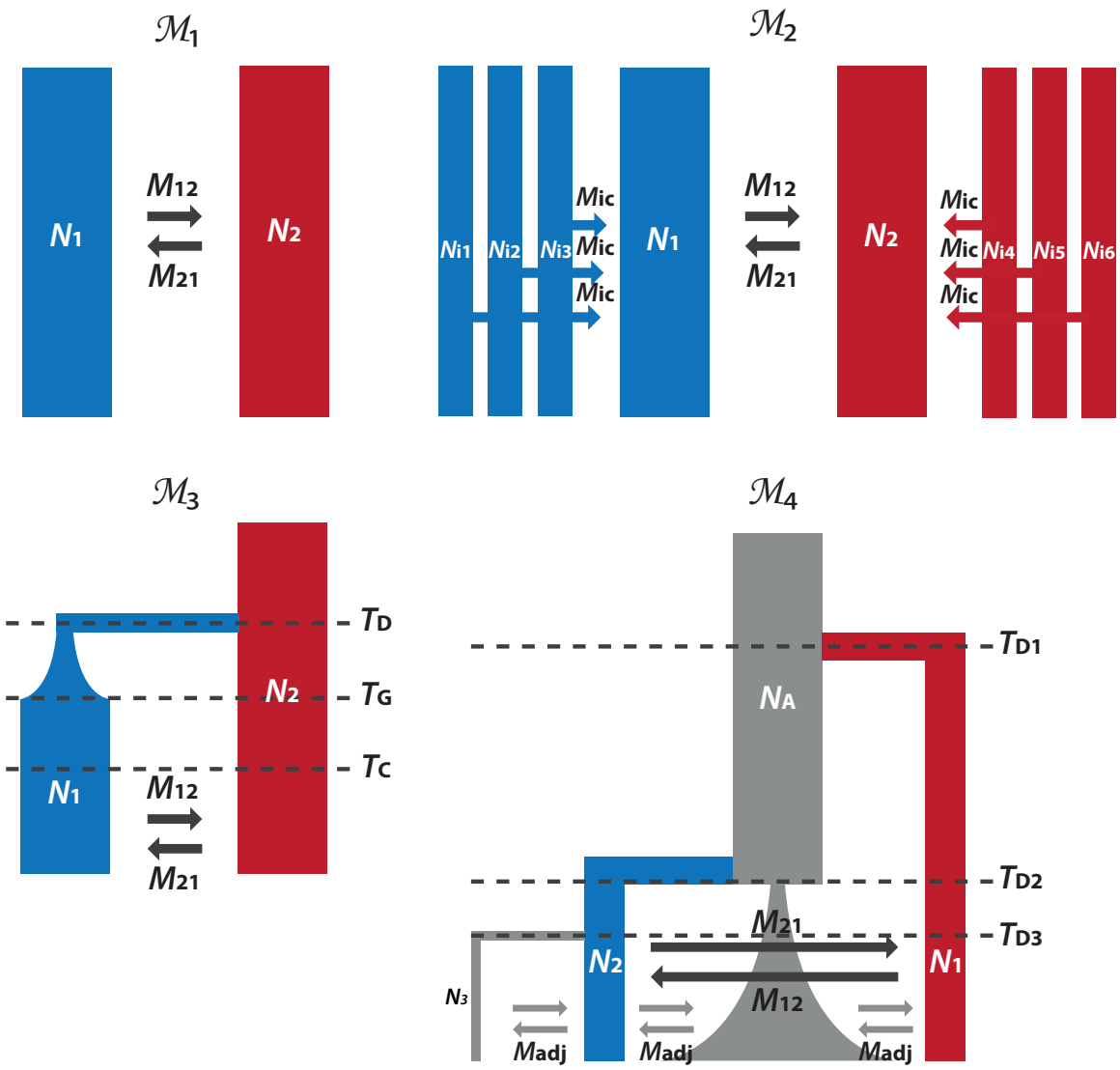

Figure 2. Models used in the simulations and case study. Model $\mathcal{M}_1$ represents a simple 2-deme isolation-with-migration (IM) model with reciprocal migration. Model $\mathcal{M}_2$ represents a 6-deme island-continent model where common differences between environments are modelled by connecting the sampled demes (i.e. islands) to respective meta-population continents via gene flow. Model $\mathcal{M}_3$ represents a 2-deme divergence with bottleneck and exponential growth model. Model $\mathcal{M}_4$ represents a 4-deme hierarchical divergence model with sequential founder events, bottleneck and exponential growth. Red and blue demes reflect contrasting environments, while grey demes reflect neutral environments where no selection acts. In all models, selection is inferred from the deviation from neutrality of the reciprocal migration rates between the two contrasting environments (M_{12}, M_{21}).

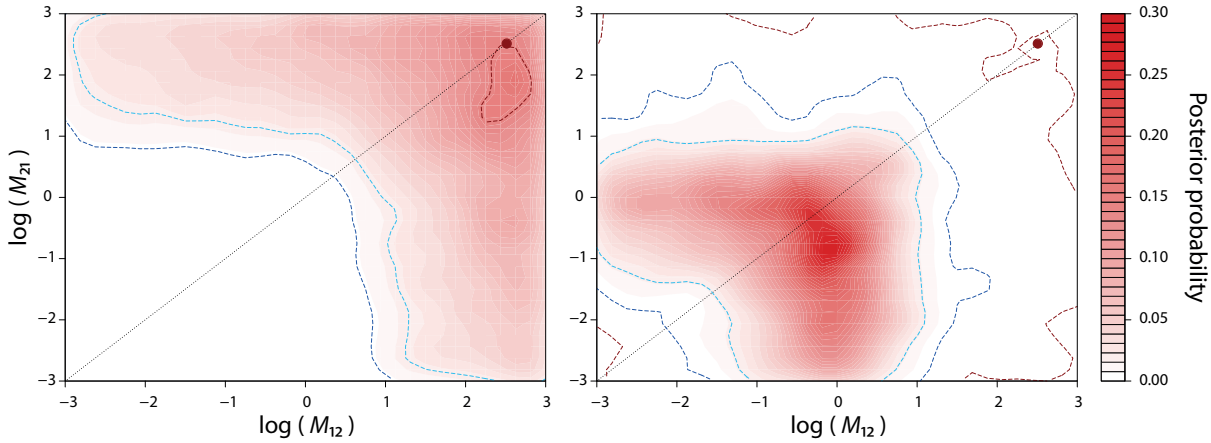

Figure 3. Exemplary joint posterior distribution of reciprocal migration parameters, M_{12} and M_{21}. The neutral joint parameter estimate, as informed by the global posterior distribution of all neutral regions (Figure S1), is indicated by the red dot in the top right corner. The red contours represent the joint posterior distribution of a genomic region (i.e. window), with the blue contours representing the 95% (light blue) and 99% (dark blue) highest density region (HDR) credible intervals. Left – a window not significantly divergent from the neutral estimate; right – a window significantly divergent from the neutral estimate, and with slightly higher relative reduction in M_{12} than in M_{21}.

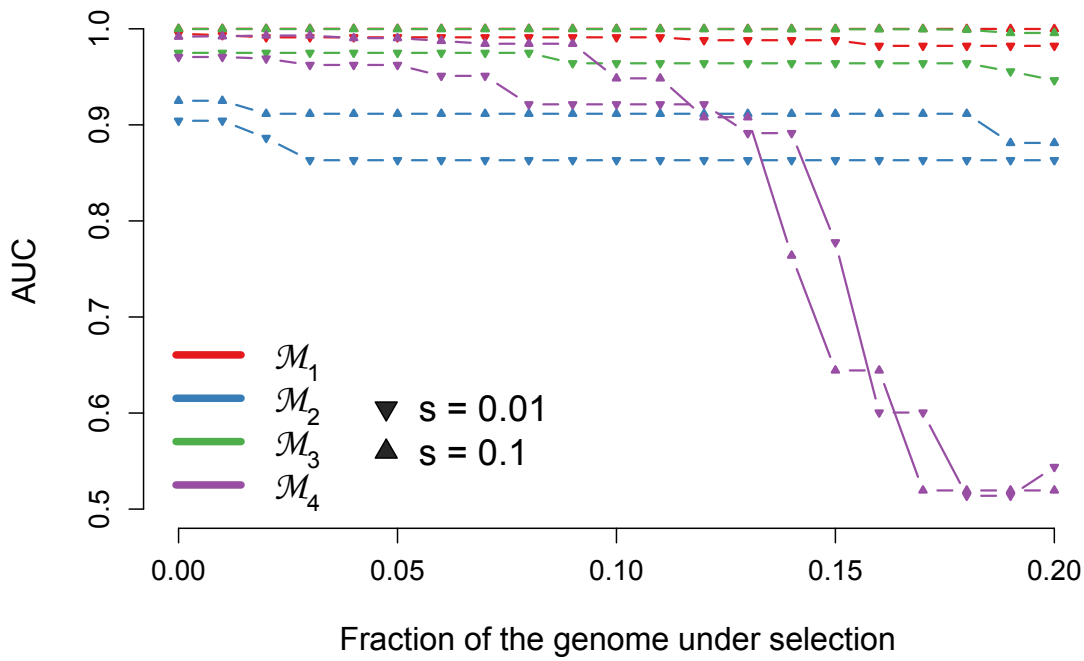

Figure 4. Effect of increasing fraction of mis-specified (aka selected) windows among the neutral set on LSD's power to detect selection, for all 4 models and intermediate and high selection coefficients ($s_1 = s_2 = s$ = 0.01, 0.1; T_S = 40,000), and under neutral migration rates

$M_{12}, M_{21} = 5$. Here the neutral set of 1000 loci comprise a fraction *f* of selected loci and a fraction 1-*f* neutral loci, with $0.0 \leq f \leq 0.2$. The selected loci comprising the pseudo-genome under scan are under the same selection regime as those included as mis-specifications in the neutral set.

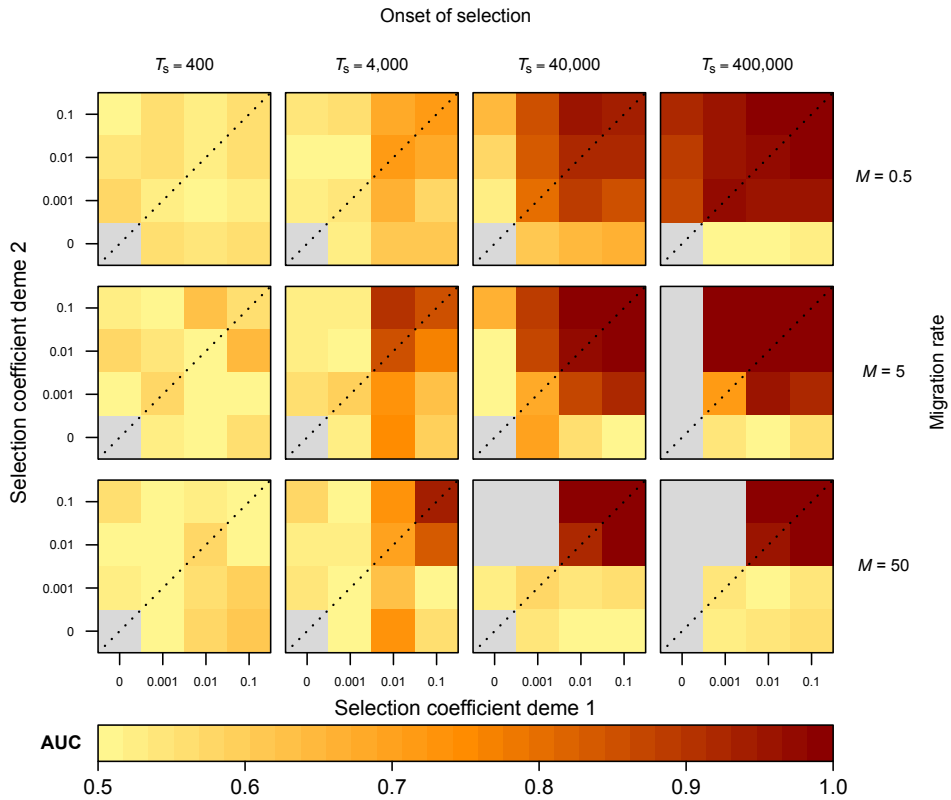

Figure 5. Simulation results showing the effect of migration rate, time of onset of selection and deme-specific selection coefficients on LSD diagnostic performance (AUC), for the 2-deme IM model (model $\boldsymbol{\mathcal{M}_1}$; standing genetic variation case). Each cell represents a pseudo-genome simulated under a specific selection regime. The cell colours reflect the AUC calculated by the correct discrimination of 1000 neutral loci and 50 selected loci in the 1050 loci simulated pseudo-genomes. Grey cells indicate selection regimes where the derived allele is always lost.

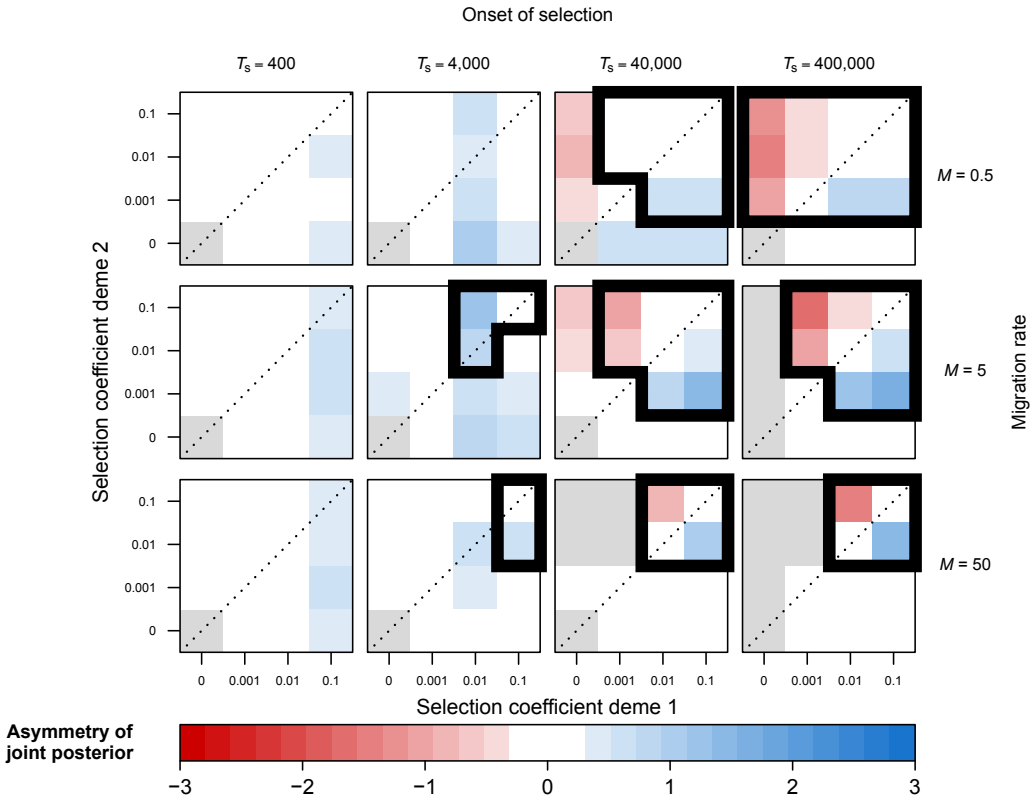

Figure 6. Simulation results showing the effect of migration rate, time of onset of selection and deme-specific selection coefficients on LSD inferred (a)symmetry of selection, for the 2-deme IM model (model $\mathcal{M}_1$; standing genetic variation case). Each cell represents a pseudo-genome simulated under a specific selection regime. The cell colours reflect the (a)symmetry values inferred by LSD, where a value of 0 reflects perfect symmetry of the joint posterior while values divergent from this reflect asymmetry. Cells surrounded by thick lines indicate the values of (a)symmetry for regimes expected to generate meaningful signal (AUC>0.8 in Figure 5). Grey cells indicate selection regimes where the derived allele is always lost.

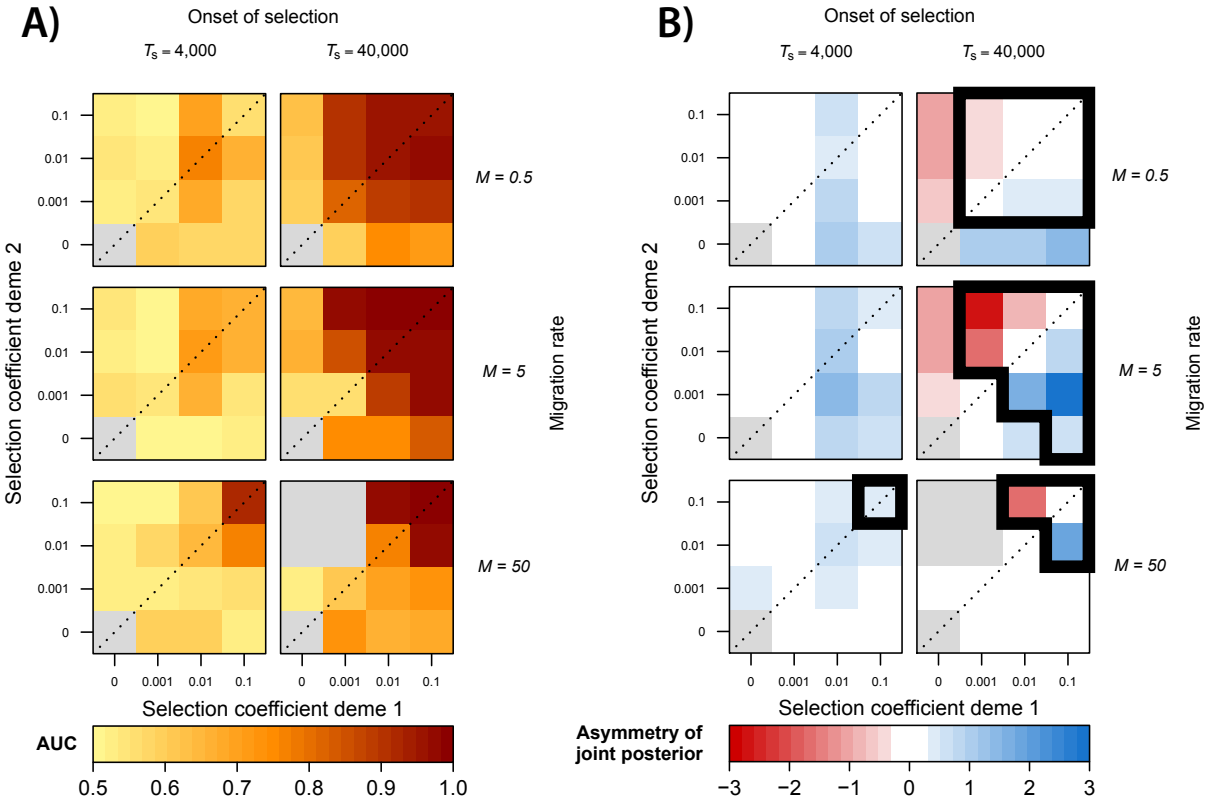

Figure 7. Simulation results for a 2-deme divergence with bottleneck and exponential growth model (model $\mathcal{M}_3$; standing genetic variation case) showing the effect of migration rate, time of onset of selection and deme-specific selection coefficients on A) LSD diagnostic performance (AUC) and B) LSD inferred (a)symmetry of selection. Divergence time of the two populations, T_D, is 200,00 generations ago. Each coloured cell represents a pseudo-genome simulated under a specific selection regime. Grey cells indicate selection regimes where the derived allele is always lost. B) Cells surrounded by thick lines indicate the values of (a)symmetry for regimes expected to generate meaningful signal (AUC>0.8 in Figure 7A).

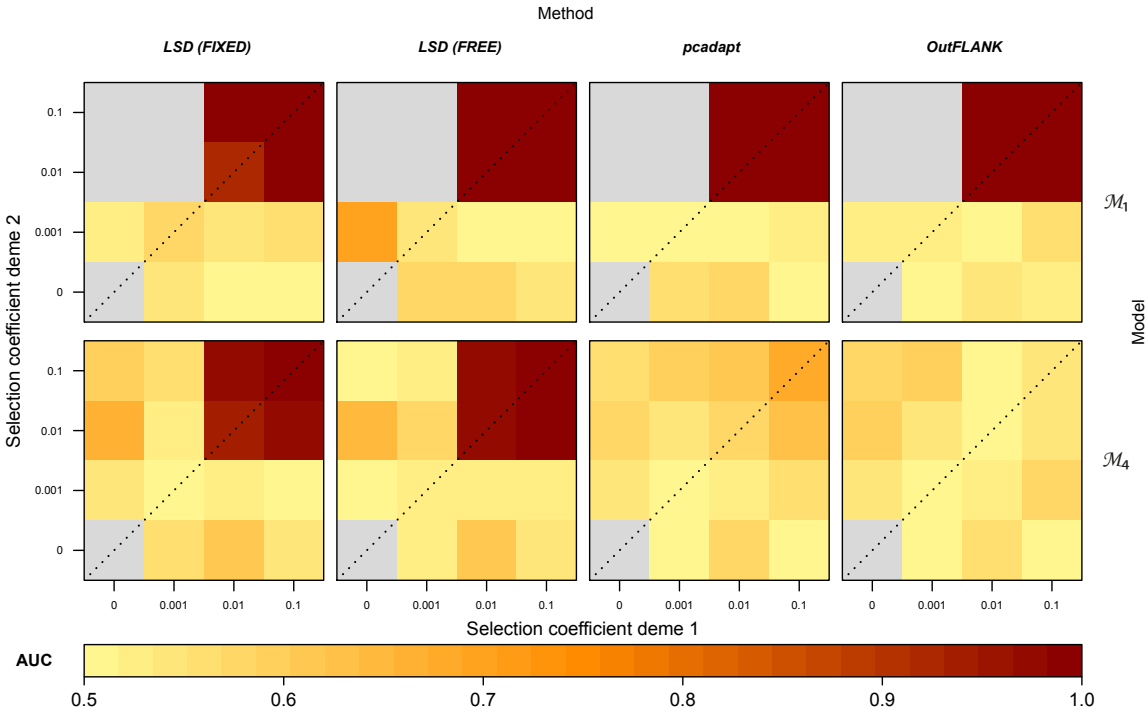

Figure 8. Comparison of power to detect selection (AUC) between LSD, pcadapt and OutFLANK. Simulation results are shown for a simple ($\boldsymbol{\mathcal{M}_1}$) and a complex demographic model ($\boldsymbol{\mathcal{M}_4}$) and for a subset of the tested migration-selection regimes at T_S = 40,000 and M = 50 (full results in Supplements). For LSD, two parametrisations are performed: i) assuming non-M demographic parameters and neutral $\widehat{M}$ to be fixed to the true values (LSD FIXED) and ii) allowing non-M demographic parameters to be drawn from large prior ranges and using neutral $\widehat{M}$ estimated from the pseudo-genomes (LSD FREE). Grey cells indicate selection regimes where the derived allele is always lost.

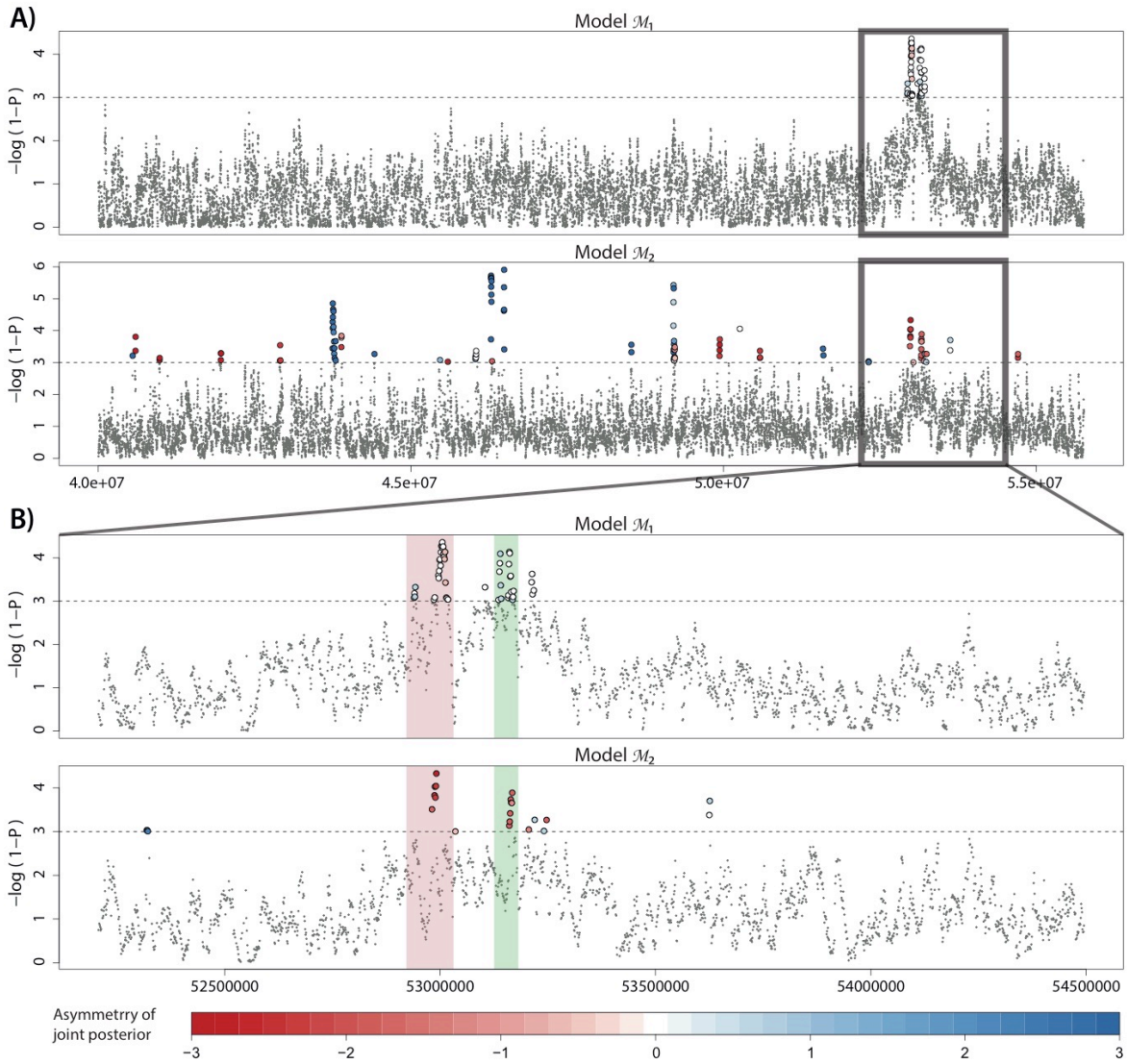

Figure 9. Manhattan plot for the LSD scan of the *A.m.striatum-A.m.pseudomajus* system. The posterior probability of observing the neutral estimate for 10kb windows (1kb step-size) is plotted for A) a 16Mb region of chromosome 6, under models $\boldsymbol{\mathcal{M}_1}$ and $\boldsymbol{\mathcal{M}_2}$, and B) a 2Mb zoomed-in region of chromosome 6 focusing on the ROS-EL region, under the same two models. The horizontal dashed line indicates a 99.9% posterior probability of deviating from neutral expectations. Colour for loci above this threshold denotes the joint (M_{12}, M_{21}) posterior (a)symmetry, and reflects the relative strengths of selection in the two divergent demes or subspecies. A large divergent peak centred around the ROS-EL region (A) is composed of a set of smaller peaks (B), consistent with the ROS (red) and EL (green) loci.

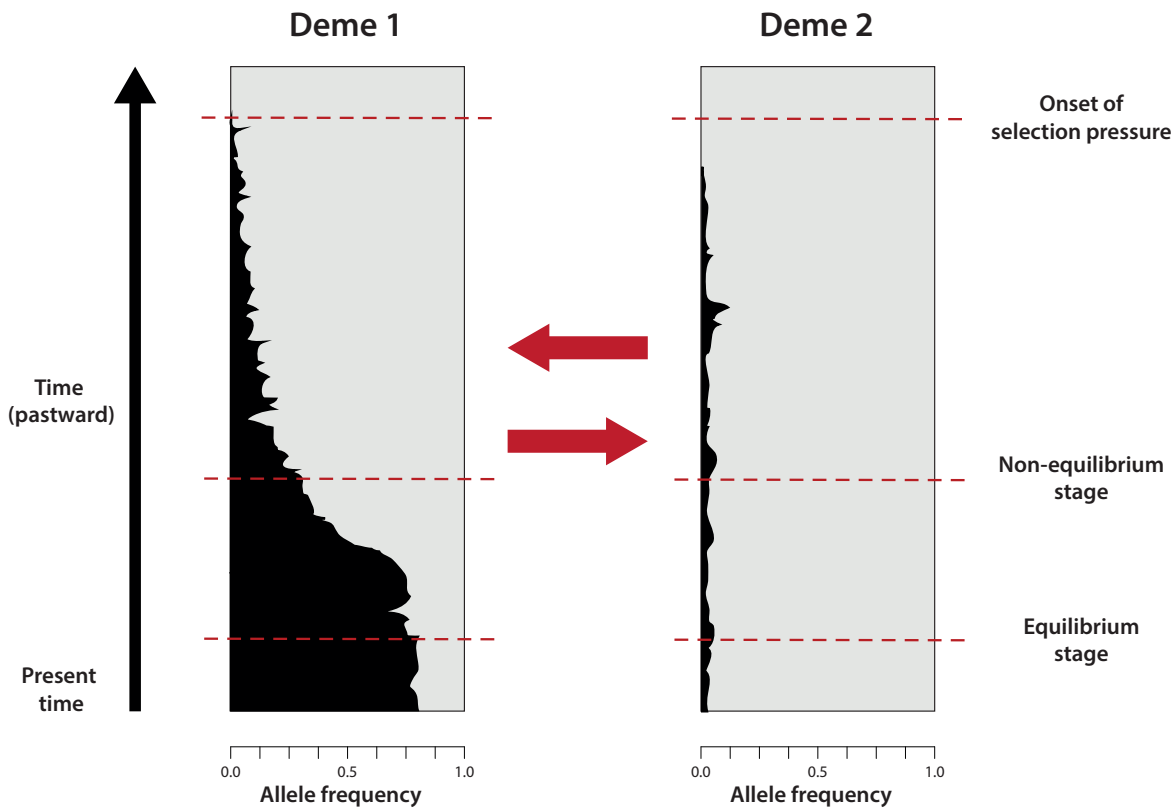

Figure 10. Conceptual illustration of allele frequency trajectories over time in a 2-deme IM model ($\mathcal{M}_1$), for an example *de-novo* case and antagonistic pleiotropic selection regime. The frequency of derived allele *A* is indicated in black and that of ancestral allele *a* in grey. Red arrows represent migration. Prior to reaching drift-migration-selection equilibrium, estimated asymmetries in effective migration rates are also affected by asymmetry in allele frequencies.